

# Crystalline Material Discovery in the Era of Artificial Intelligence

Zhenzhong Wang<sup>1,\*</sup>, Haowei Hua<sup>1,\*</sup>, Wanyu Lin<sup>1,2,†</sup>, Ming Yang<sup>3</sup>, and Kay Chen Tan<sup>2</sup>

<sup>1</sup>The Hong Kong Polytechnic University, Department of Computing

<sup>2</sup>The Hong Kong Polytechnic University, Department of Data Science and Artificial Intelligence

<sup>3</sup>The Hong Kong Polytechnic University, Department of Applied Physics

<sup>†</sup>Corresponding author. Email: wan-yu.lin@polyu.edu.hk;

\*These authors contributed equally to this work.

## ABSTRACT

Crystalline materials, with symmetrical and periodic structures, exhibit a wide spectrum of properties and have been widely used in numerous applications across electronics, energy, and beyond. For crystalline materials discovery, traditional experimental and computational approaches are time-consuming and expensive. In these years, thanks to the explosive amount of crystalline materials data, great interest has been given to data-driven materials discovery. Particularly, recent advancements have exploited the expressive representation ability of deep learning to model the highly complex atomic systems within crystalline materials, opening up new avenues for fast and accurate materials discovery. These works typically focus on four types of tasks, including physicochemical property prediction, crystalline material synthesis, aiding characterization, and accelerating theoretical computations. Despite the remarkable progress, there is still a lack of systematic investigation to summarize their distinctions and limitations. To fill this gap, we systematically investigated the progress made in recent years. We first introduce several data representations of the crystalline materials. Based on the representations, we summarize various fundamental deep learning models and their tailored usages in various material discovery tasks. Finally, we highlight the remaining challenges and propose future directions.

## 1 Introduction

Crystalline materials, possessing unique structures and diverse properties, have been the cornerstone of a wide range of applications such as electronics, sustainable energy, etc<sup>1-6</sup>. They are arranged periodically in the units —*crystal lattice*. Within the crystal lattice, the atoms are arranged meticulously with symmetrical structures, establishing uniform atomic interactions. The long-range order characterized by periodicity and the short-range order featured by symmetry gives rise to their structural stability<sup>7-9</sup>. These distinctive structures also induce a diverse array of physical and chemical properties, enabling the versatility of crystalline materials.

The development of new crystalline materials with desired properties is a fundamental problem, which requires a deep understanding of structure-property relationships behind the materials<sup>10-12</sup>. To uncover the structure-property relationships, hitherto, material science has gone through four paradigms<sup>13</sup>. Before the 17th century, material science primarily relied on empirical and observational methods. In the 17th century, the advent of calculus initiated the second scientific revolution, a transition to theoretical science, characterized by mathematical equations of natural phenomena. The invention of computers in the 20th century created the third paradigm, the computational science paradigm, enabling larger and more complex theoretical equations to become solvable. Through computational simulations, e.g., density functional theory (DFT), new materials can be tested and evaluated. However, due to the vast chemical space of compositions and structures, using these simulations to explore the structure-property relationships is of high computational cost and highly depends on the trial-and-error approaches<sup>9,13,14</sup>.

In recent years, the fourth paradigm — Artificial Intelligence (AI)-powered materials science<sup>4,15,16</sup>, provides a new avenue for material discovery. Especially, deep learning techniques have revolutionized the field of materials science, enabling the rapid discovery of new materials. One of the key drivers is the availability of large datasets from experiments and simulations<sup>17-19</sup>. For example, the Materials Project database includes property calculations for over 60,000 molecules and over 140,000 inorganic compounds of clean energy systems such as photovoltaics, thermoelectric materials, and catalysts<sup>20</sup>. Additionally, the Open Catalyst Project (OCP) has made available a vast dataset of crystal structures, consisting of 1.3 million structural relaxations with results from over 260 million DFT calculations<sup>21</sup>. More recently, the OMat24 database contains over 110 million DFT calculations, focusing on structural and compositional diversity<sup>22</sup>.

These explosive growths of data have filled the fuel for AI-driven materials science. With these abundant data, deep learning has provided fresh perspectives on various tasks for crystalline material discovery, including physicochemical property

prediction, crystalline material synthesis, aiding characterization, and accelerating theoretical computations. *Physicochemical property prediction* is a fundamental task in deep learning-driven materials science, where the goal is to predict a material's physical and chemical properties. These models typically take the crystal structure as input and output the predicted properties, including scalar properties and tensor properties<sup>23–31</sup>. *Crystalline material synthesis* is to discover new crystal materials including new compositions and structures. The newly discovered material requires not only stability but also specific properties<sup>9,26,27,32</sup>. *Aiding characterization* is to use deep learning models to aid the quantitative or qualitative analysis of experimental observations and measurements, including assisting in the determination of crystal structure and composition, identifying structural transition, and inferring crystal symmetry and defects<sup>33–39</sup>. *Accelerating theoretical computations* aim to reduce the computational cost of intractable simulations by using deep learning models as surrogates to provide potentials, functionals, and electronic structures<sup>40–43</sup>.

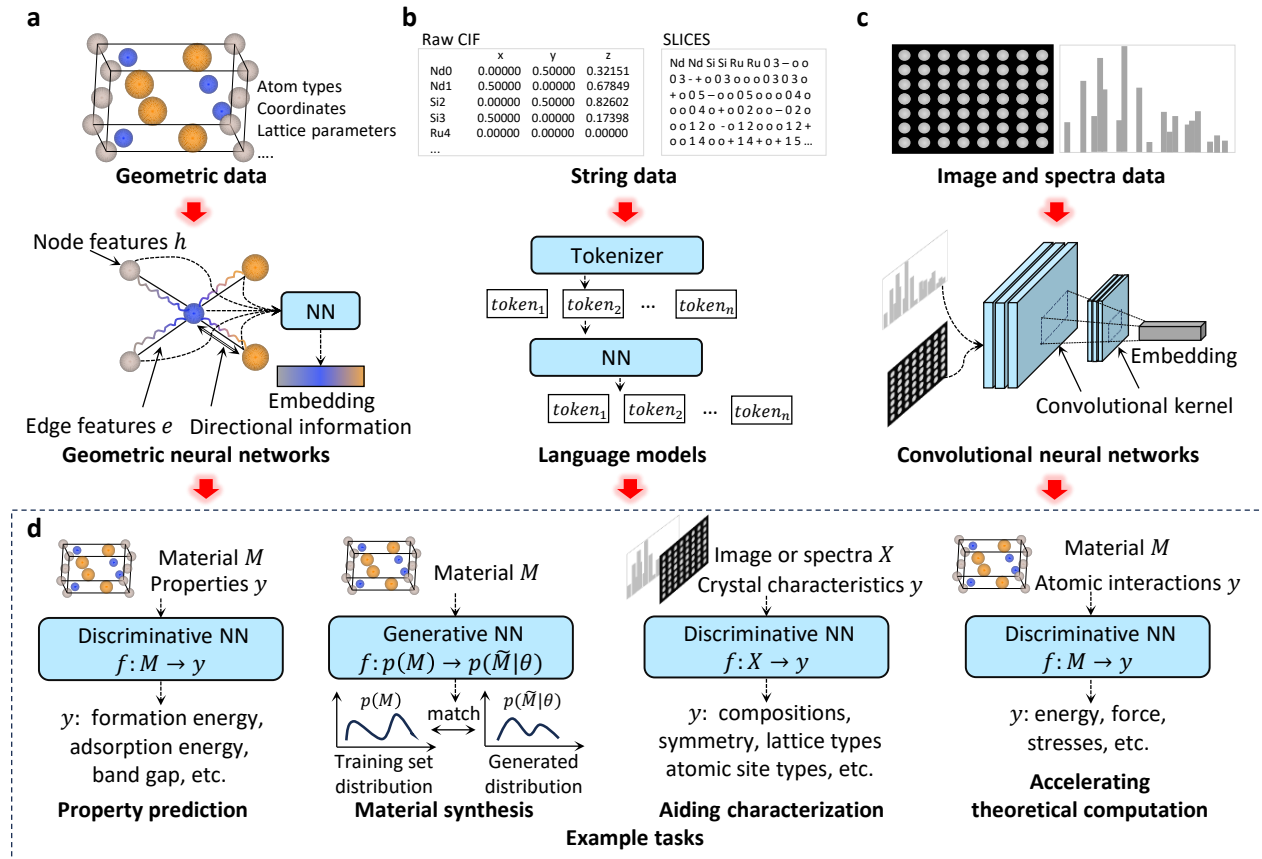


**Figure 1. Overview of deep learning for crystalline materials.** **a** Crystalline materials are described by geometric graphs. Typically, geometric graph neural networks are used to extract atom, bond, and directional information from the geometric graphs based on message-passing mechanisms. **b** Language models are generally used to handle the string representations, such as CIF and SLICES<sup>44</sup>. **c** The atomic image and spectra data of crystalline materials are processed using convolutional neural networks; the convolutional kernels transform these data into feature map representations. **d** The above fundamental models serve as surrogates for various material discovery tasks, including physicochemical property prediction, crystalline material synthesis, aiding characterization, and accelerating theoretical computations.

In this review, we will investigate how AI, especially deep learning techniques, leverages various crystalline material data to learn from crystalline materials for realizing the above four fundamental tasks. While several existing reviews have discussed related topics<sup>35,45</sup>, they neither cover recently emerged deep learning methodologies for crystalline materials nor have comprehensive coverage of concepts and related tasks to crystalline materials. Our review distinguishes itself by fulfilling a dual purpose: it functions as both an accessible tutorial introducing fundamental concepts of crystalline materials and state-of-the-art deep learning methodologies, and as a detailed guide to current research developments, highlighting distinctions, advances, and limitations in the domain. Through this dual approach, we aim to provide readers with a broad conceptual overview that bridges AI and materials science, fostering deeper insights into this interdisciplinary field.

In the review, we provide several data representations that have been used in crystalline material research. The data

representations involve geometric graphs, string representations, images, and spectra, as shown in FIG. 1a, b, and c. With different data representations, various fundamental models such as geometric graph neural networks<sup>46,47</sup>, language models<sup>48,49</sup>, and convolutional neural networks<sup>50,51</sup> and their design principles are introduced. Then, we mainly focus on the recently proposed deep learning models on physicochemical property prediction, crystalline material synthesis, aiding characterization, and accelerating theoretical computations, as shown in FIG. 1d. In addition, we provide some of the commonly used datasets, benchmarks, and software used for data-driven crystalline material discovery. It is worth noting that while deep learning has shown its potential in facilitating the development of crystalline material discovery, many challenges and issues need to be addressed to unleash the potential of deep learning for crystalline materials further. Therefore, we also highlight these challenges and provide insights in this domain. This review aims to offer comprehensive and valuable insights, and fosters progress in the intersection of artificial intelligence and material science. We have organized the surveyed work and benchmarking, which can be accessed via the following link: <https://github.com/WanyuGroup/AI-for-crystal-materials/>.

## 2 Data Representations Describing Crystalline Materials

Crystalline materials are inherently organized with a periodic arrangement of atoms in the 3D space. The periodic unit, known as the unit cell, is defined by the lattice parameters, which are the lengths of the cell edges and the angles between them. Within the unit cell, an array of atoms is arranged, each of which is defined by its type and atomic coordinates. Traditionally, the above information on crystalline materials is documented in text-based formats, namely Crystallographic Information Files (CIFs). CIFs have been the *de facto* data representation of crystalline materials<sup>52</sup>, as they record the detailed information about a crystal structure, including atom types, atomic coordinates, lattice parameters, space groups, and other structural attributes as illustrated in FIG. 2a. Several studies simply use CIFs as the string input and employ language models for various downstream tasks<sup>27,53</sup>. By extracting and interpreting the geometric data from these CIFs, one can generate 3D geometric graphs that accurately represent the overall crystal structures. In addition, researchers can also employ advanced imaging techniques and electromagnetic radiation to obtain atomic images and spectroscopic data. In this regard, this section will provide an overview of commonly used data representations for crystalline materials.

### 2.1 Strings

The simplified line-input crystal-encoding system (SLICES) attempts to provide invertible, invariant, periodicity-aware text-based representations for crystalline materials<sup>44</sup>. A quotient graph was proposed to serve as an intermediary to transform between the crystal structures and the SLICES strings<sup>54</sup>. The quotient graph indicates how atoms in a unit cell are connected to atoms within the adjacent unit cells. For instance, as depicted in FIG. 2c, the edge  $e_4$  labeled "0 0 1" in the quotient graph, indicates that  $e_4$  connects node  $C_0$  to the copy of  $C_1$  shifted one unit along the  $c$  axis.

SLICES strings convert the quotient graph into three components: atomic symbols, node indices, and edge labels. Specifically, a SLICES string begins with the atomic symbols of the unit cell, encoding the chemical composition of the crystal structure. Edges are explicitly represented in the form  $uvxyz$ , where  $u$  and  $v$  are node indices, and  $xyz$  denotes the location of the unit cell to connect to. To represent the quotient graph in FIG. 2c, the SLICES string begins with atom symbols  $C_0$  and  $C_1$  of node indices 0 and 1, respectively. Following the atom symbols, the edges  $e_1 \dots e_4$  of the form  $uvxyz$  in the quotient graph are appended. For example,  $e_4$  is represented as "01oo+". Here, 01 denotes the atomic indices corresponding to the positions in the atomic symbols of the SLICES string (i.e.  $C_0$  and  $C_1$ ). The sequence "oo+" represents the label "0 0 1" from the labeled quotient. To reconstruct the original crystal structures from the SLICES strings, Eon's graph theory<sup>55</sup> and force field approaches, including geometry frequency noncovalent force field<sup>56</sup> and M3GNet<sup>41</sup>, can be used to ensure invertibility. On the Materials Project dataset<sup>20</sup>, the reconstruction routine of SLICES can successfully reconstruct 94.95% of 40,000 crystal structures which are structurally and chemically diverse, showcasing an unprecedented invertibility.

### 2.2 Geometric Graphs

With the geometric details of crystalline materials provided in CIFs, it is feasible to model geometric graphs of these materials within the 3D Euclidean space, as shown in FIG. 2b. Next, we introduce two widely utilized coordinate systems, namely the Cartesian coordinate system and the fractional coordinate system. These two coordinate systems are fundamental tools for representing the geometric configuration of crystalline materials<sup>57,58</sup>. Furthermore, based on the corresponding coordinate systems, we will introduce two important concepts in crystal research: the space group and the Wyckoff positions.

**Cartesian Coordinate System.** A crystalline material can be formally represented as  $\mathbf{M} = (\mathbf{A}, \mathbf{X}, \mathbf{L})$ , where  $\mathbf{A} = [\mathbf{a}_1, \mathbf{a}_2, \dots, \mathbf{a}_n]^T \in \mathbb{R}^{n \times d_a}$  denotes the atom feature matrix for  $n$  atoms within a unit cell, with  $\mathbf{a}_i \in \mathbb{R}^{d_a}$  representing the  $d_a$ -dimensional feature vector of an individual atom, such as the atomic type. The matrix  $\mathbf{X} = [\mathbf{x}_1, \mathbf{x}_2, \dots, \mathbf{x}_n]^T \in \mathbb{R}^{n \times 3}$  represents the 3D Cartesian coordinates of  $n$  atoms within a unit cell, where  $\mathbf{x}_i \in \mathbb{R}^3$  specifies the Cartesian coordinates of each atom. The repeated patterns of a crystal material can be described by the lattice matrix  $\mathbf{L} = [\mathbf{l}_1, \mathbf{l}_2, \mathbf{l}_3] \in \mathbb{R}^{3 \times 3}$ , where  $\mathbf{l}_1$ ,  $\mathbf{l}_2$ , and  $\mathbf{l}_3$  are a set of basis vectors in the 3D Euclidean space. The unit cell repeats itself along three basis vector directions to

form a complete crystal. Finally, a complete crystal can be represented as  $(\hat{\mathbf{A}}, \hat{\mathbf{X}}) = \{(\hat{\mathbf{a}}_i, \hat{\mathbf{x}}_i) | \hat{\mathbf{x}}_i = \mathbf{x}_i + k_1 \mathbf{l}_1 + k_2 \mathbf{l}_2 + k_3 \mathbf{l}_3, \hat{\mathbf{a}}_i = \mathbf{a}_i, k_1, k_2, k_3 \in \mathbb{Z}, i \in \mathbb{Z}, 1 \leq i \leq n\}$ . The integers  $k_i$  and  $l_i$  represent all possible atomic positions in the periodic lattice.

**Fractional Coordinate System.** The fractional coordinate employs  $\mathbf{L} = [\mathbf{l}_1, \mathbf{l}_2, \mathbf{l}_3] \in \mathbb{R}^{3 \times 3}$  as the basis vectors for atomic positions. The position of an atom can be described with a fractional coordinate vector  $\mathbf{f}_i = [f_1, f_2, f_3]^T \in [0, 1)^3$ . The corresponding Cartesian coordinate vector can be expressed as  $\mathbf{x}_i = \mathbf{f}_i \mathbf{l}_i$ . Therefore, a crystal  $\mathbf{M}$  can be represented as  $\mathbf{M} = (\mathbf{A}, \mathbf{F}, \mathbf{L})$ , where  $\mathbf{F} = [\mathbf{f}_1, \dots, \mathbf{f}_n]^T \in [0, 1)^{n \times 3}$  represents the fractional coordinates of all atoms in the unit cell.

**Space Group.** When we rotate and translate the 3D crystal structures in the 3D space, certain rotation angles and translation distances can map a crystal structure back onto itself due to the inherent symmetry of the structure. These specific rotation and translation transformations are collectively defined as space groups. Specifically, given a group  $g \in E(3)$  (See Box 1), a crystal  $\mathbf{M}$  is recognized to be symmetric with respect to  $g$  if  $g \cdot \mathbf{M} = \mathbf{M}$  (the symbol  $=$  here refers to the equivalence between geometric structures). The set of all possible  $g$  constitutes the space group of  $\mathbf{M}$ , and the total number of different space groups is finite. Accordingly, space groups are classified into 230 types for 3D crystal structures<sup>60,61</sup>. The finite space group also imposes strict constraints on specific positions of atoms within the crystal structure, known as Wyckoff positions.

**Wyckoff Positions.** Wyckoff positions describe a set of symmetry-equivalent positions within the unit cell<sup>27,60,62</sup>, which are determined by the space group transformations. Generally, Wyckoff positions include three elements: multiplicity, Wyckoff letter, and fractional coordinates. For instance, FIG. 2e shows the Wyckoff positions for the 2D plain group P4mm<sup>61</sup>. These Wyckoff positions are labeled using Wyckoff letters from the alphabet, which represent distinct symmetry-equivalent sites. The multiplicity indicates the number of these symmetry-equivalent sites. To preserve the symmetry of the crystal structure, all these positions must be occupied by the same type of atoms. In FIG. 2e,  $x$  and  $y$  are fractional coordinates, where  $0 \leq x \leq 0.5; 0 \leq y \leq 0.5; x \leq y$ . FIG. 2f presents a schematic diagram of the Wyckoff positions, with symmetry-equivalent positions marked by the same color.

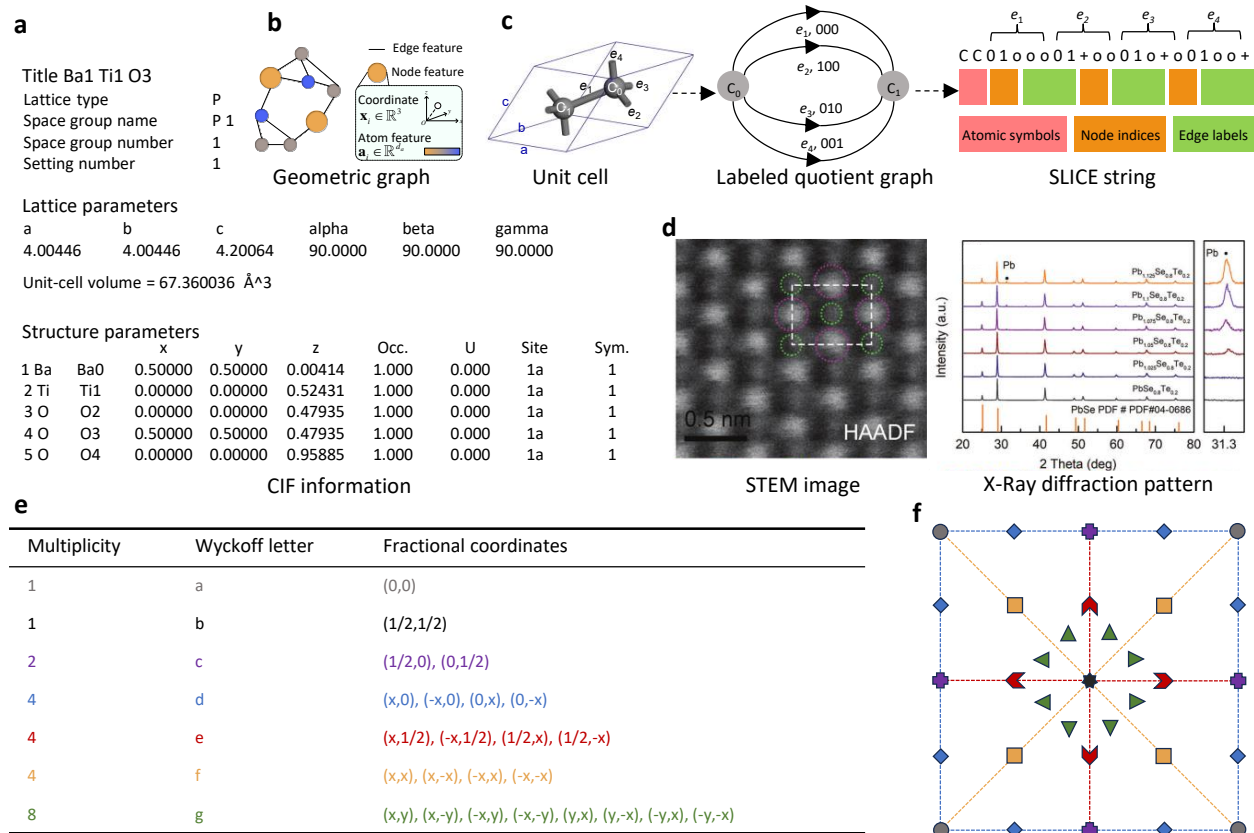


**Figure 2. Examples of data representations: strings, images, and spectra data.** **a** | The CIF of BaTiO<sub>3</sub> (MP ID: mp-5986, from the Materials Project<sup>20</sup>). **b** | The geometric graph representation. **c** | The illustration of SLICES string conversion process. **d** | The scanning transmission electron microscopy image and the X-ray diffraction spectra data. **e** | The Wyckoff positions of the P4mm space group (No.11). **f** | The schematic diagram for the Wyckoff positions of the P4mm space group. Panel **c** adapted from REF.<sup>44</sup>. Panel **d** adapted from REF.<sup>59</sup>.

## 2.3 Images

Crystalline material image representations are obtained through various advanced imaging techniques, such as diffraction imaging and microscopy<sup>33–35,63</sup>. Representative diffraction imaging methods include X-ray diffraction (XRD), electron diffraction, and neutron diffraction<sup>64–67</sup>. Microscopy techniques have many different imaging modalities, including scanning transmission electron microscopy (STEM), scanning probe microscopy (SPM), and transmission electron microscopy (TEM)<sup>68–71</sup>. For example, STEM images, are shown in FIG. 2d, can reflect the surface morphology and the structure of crystalline materials. These image representations are instrumental in executing specific tasks such as defect detection and classification<sup>33,34</sup>.

## 2.4 Spectra

The interaction between electromagnetic radiation and materials can generate a measurable spectroscopic signal that varies with the radiation's wavelength or frequency. The spectroscopic signal, generally referred to as *spectra data*, is commonly acquired through X-ray diffraction (XRD) and Raman spectroscopy<sup>35–37</sup>. As depicted in FIG. 2d, XRD spectra present the plots of X-ray intensity versus the diffraction angle. Therefore, XRD spectra can provide quantitative information about the crystal structure parameters such as peak positions and intensities, which correspond to interplanar spacings and crystallite sizes. On the other hand, the Raman spectra, obtained by measuring the frequency shift of scattered light, can provide characteristic information about crystal structures. This spectral data is instrumental in identifying intrinsic material properties such as chemical composition and crystallographic details<sup>72,73</sup>.

# 3 Fundamental Deep Learning Models

In this section, we will present fundamental deep learning models, including geometric graph neural networks (GGNNs), convolutional neural networks (CNNs), language models, and diffusion models. These deep learning models have played a cornerstone role in recent advancements.

## 3.1 Geometric Graph Neural Networks

GGNNs are specifically designed to handle the complex geometric relationships within the geometric graph data, such as proteins, molecules, and crystalline materials<sup>9,74–76</sup>. The key design principles of GGNNs are rooted in the principles of message-passing and aggregation mechanisms. The message-passing mechanism processes graph-structured data by exchanging each node's information with its neighboring nodes through edges. The aggregation performs local updates to node features by aggregating information from its immediate neighbors. Formally, the entire process can be expressed as follows<sup>77</sup>:

$$m_{ij} = \phi_{\text{msg}}(h_i^{(l-1)}, h_j^{(l-1)}, d_{ij}, e_{ij}), \quad h_i^{(l)} = \phi_{\text{agg}}(h_i^{(l-1)}, \{m_{ij}\}_{j \in \mathcal{N}_i}), \quad (1)$$

where  $\phi_{\text{msg}}(\cdot)$  and  $\phi_{\text{agg}}(\cdot)$  represent the message calculation and aggregation, respectively,  $h_i^{(l-1)}$  and  $h_j^{(l-1)}$  are the node features of the  $i$ -th and  $j$ -th nodes in the  $(l-1)$ -th layer, respectively,  $h_i^{(l)}$  represents the node feature of the  $i$ -th node in the  $l$ -th layer,  $d_{ij} = \|x_i - x_j\|^2$  is the directional information between the node coordinates  $x_i$  and  $x_j$ ,  $e_{ij}$  denotes the edge features, and  $m_{ij}$  represents the computed message.

Noticeably, compared to the vanilla message-passing mechanism in graph neural networks, Eq. (1) also encodes the directional information  $d_{ij}$  between two nodes (angle information can also be included). By integrating this geometric information, GGNNs can perceive the symmetry inherent in crystalline materials. This capability allows GGNNs to preserve equivariance or invariance to group transformations such as translations, rotations, and reflections, which ultimately enhances the model's generalization ability and robustness. Box 1 provides the concepts of group transformations, equivariance, and invariance, respectively.

### Box 1 | Group, Equivariance and Invariance.

#### Group

A group  $G$  is a set of transformations with a binary operation " $\cdot$ " that satisfies the following properties:

- (i) Closure:  $\forall a, b \in G, a \cdot b \in G$ ;
- (ii) Associativity:  $\forall a, b, c \in G, (a \cdot b) \cdot c = a \cdot (b \cdot c)$ ;
- (iii) Identity element: there exists an identity element  $e \in G$  such that  $\forall a \in G, a \cdot e = e \cdot a = a$ ;
- (iv) Inverses: there exists an identity element  $e \in G$  such that  $\forall a \in G, \exists b \in G, a \cdot b = b \cdot a = e$ , where the inverse  $b$  is denoted as  $a^{-1}$ .

Here are some groups commonly used in crystalline materials research.

1.  $E(d)$  is an Euclidean group comprising rotations, reflections, and translations, acting on  $d$ -dimension vectors.

2.  $O(d)$  is an orthogonal group, consisting of rotations and reflections, acting on  $d$ -dimension vectors.
3.  $SE(d)$  is a special Euclidean group, which includes only rotations and translations.
4.  $SO(d)$  is a special orthogonal group, consisting exclusively of rotations.
5.  $S_N$  is a permutation group, whose elements are permutations of a given set consisting of  $N$  elements.

### Equivariance

A function  $f: \mathcal{X} \rightarrow \mathcal{Y}$  is  $G$ -equivariant if applying a group transformation to the input results in the same transformation applied to the output:  $\phi(g \cdot x) = g \cdot \phi(x), \forall g \in G$ . With group representation, this becomes:  $\phi(\rho_{\mathcal{X}}(g)x) = \rho_{\mathcal{Y}}(g)\phi(x), \forall g \in G$ , where  $\rho_{\mathcal{X}}(\cdot)$  and  $\rho_{\mathcal{Y}}(\cdot)$  are the group representations in the input and output spaces, respectively.

### Unit Cell E(3) Equivariance

For crystalline materials, if  $f: (\mathbf{A}, \mathbf{X}, \mathbf{L}) \rightarrow \mathcal{Y}$  is unit cell  $E(3)$ -equivariant, then:  $\mathbf{Q}f(\mathbf{A}, \mathbf{X}, \mathbf{L}) = f(\mathbf{A}, \mathbf{Q}\mathbf{X} + \mathbf{b}, \mathbf{Q}\mathbf{L})$ , where  $\mathbf{Q}$  is a rotation matrix and  $\mathbf{b}$  is a translation vector.

### Permutation Equivariance

If function  $f: (\mathbf{A}, \mathbf{X}, \mathbf{L}) \rightarrow \mathcal{Y} \in \mathbb{R}^n$  is permutation equivariant, then we have  $\mathbf{P}f(\mathbf{A}, \mathbf{X}, \mathbf{L}) = f(\mathbf{P}\mathbf{A}, \mathbf{P}\mathbf{X}, \mathbf{L})$ , where  $\mathbf{P} \in \{0, 1\}^{n \times n}$  is a permutation matrix (represent the operation of adjusting the atom order).

### Invariance

Similar to equivariance, a function  $f: \mathcal{X} \rightarrow \mathcal{Y}$  is  $G$ -invariant if applying a group transformation to the input leaves the output unchanged:  $\phi(g \cdot x) = \phi(x), \forall g \in G$ . With group representation, this becomes:  $\phi(\rho_{\mathcal{X}}(g)x) = \phi(x), \forall g \in G$ .

### Unit Cell E(3) Invariance

We particularly consider the invariance of unit cells. For a function  $f: (\mathbf{A}, \mathbf{X}, \mathbf{L}) \rightarrow \mathcal{Y}$ , if it is invariant under the  $E(3)$  group, then we have  $f(\mathbf{A}, \mathbf{X}, \mathbf{L}) = f(\mathbf{A}, \mathbf{Q}\mathbf{X} + \mathbf{b}, \mathbf{Q}\mathbf{L})$ , where  $\mathbf{Q} \in \mathbb{R}^{3 \times 3}$  is a rotation and reflection matrix and  $\mathbf{b} \in \mathbb{R}^3$  is a translation vector.

### Permutation Invariance

Similarly, we consider the permutation invariance w.r.t the atom order. If function  $f: (\mathbf{A}, \mathbf{X}, \mathbf{L}) \rightarrow \mathcal{X}$  is permutation invariant, then we have  $f(\mathbf{A}, \mathbf{X}, \mathbf{L}) = f(\mathbf{P}\mathbf{A}, \mathbf{P}\mathbf{X}, \mathbf{L})$ , where  $\mathbf{P}$  is a permutation matrix.

### Periodic Invariance

For periodic crystal data, scaling or shifting the unit cell leads to different representations for the same crystal. Consequently, models applied to crystal data also need to be periodic invariant. If a function  $f: (\mathbf{A}, \mathbf{X}, \mathbf{L}) \rightarrow \mathcal{X}$  exhibits periodic invariance,  $f(\mathbf{A}, \mathbf{X}, \mathbf{L}) = f(\Phi(\hat{\mathbf{A}}, \hat{\mathbf{X}}, \alpha\mathbf{L}, \mathbf{p}), \alpha\mathbf{L})$ , where  $\Phi: (\hat{\mathbf{A}}, \hat{\mathbf{X}}, \mathbf{L}, \mathbf{p}) \rightarrow (\mathbf{A}, \mathbf{X})$  represents the abstract generating function of the unit cell and  $\mathbf{p}$  is a corner point.  $\alpha \in \mathbb{N}_+^3$  is a scalar that pertains to the scaling of unit cell size.

## 3.2 Convolutional Neural Networks

CNNs have revolutionized the field of deep learning, particularly in vision domains. In recent years, CNNs have also been applied to atomic image-based aiding characterization tasks such as structure recognition, defect detection, and microstructure analysis<sup>33,34,78,79</sup>. A typical CNN architecture consists of several key components, including convolution layers, pooling layers, activation functions, and fully connected layers. Convolutional layers aim to autonomously detect spatial hierarchies within data. Specifically, convolutional operations involve sliding a convolutional kernel over the input data to compute local patterns. This process enables the CNNs to learn features from small local regions and progressively capture more complex patterns as the network deepens. Following the convolutional layers, pooling layers are used to downsample the feature maps, retaining the most critical information while reducing dimensionality. Common pooling methods include max pooling and average pooling, both of which help mitigate overfitting and decrease computational load. CNNs incorporate activation functions like ReLU to introduce non-linearity into the model. In standard CNN architectures, the final layers are fully connected layers, which use the high-level features learned by the convolutional and pooling layers to make final predictions.

## 3.3 Language Models

The evolution of language models within the domain of deep learning has witnessed remarkable progress over the past decade, particularly in the field of natural language processing<sup>80-82</sup>. With the emergence of chemical languages, e.g., simplified molecular input line entry systems (SMILES<sup>83</sup>), language models have also demonstrated tremendous potential in the field of science. Current mainstream language models primarily rely on transformer architectures which consist of an encoder and a decoder. The encoder's role is to convert an input sequence into a fixed-length vector, or embedding. This embedding serves as a comprehensive representation, encapsulating both short- and long-range dependencies within the data. The decoder subsequently leverages this embedding to generate the output sequence. The core innovation of the transformer is the self-attention mechanism. This allows the model to weigh the significance of different input tokens in a sequence relative to one another. By calculating attention scores, the model can focus on particular parts of the input, enabling it to capture

contextual relationships without relying on sequential processing. Specifically, through defining three learnable weight matrices  $\mathbf{W}_Q \in \mathbb{R}^{d \times d_q}$ ,  $\mathbf{W}_K \in \mathbb{R}^{d \times d_k}$ , and  $\mathbf{W}_V \in \mathbb{R}^{d \times d_v}$ , the input embeddings  $\mathbf{X} \in \mathbb{R}^{n \times d}$  are linearly transformed to three parts, i.e., queries  $\mathbf{Q} \in \mathbb{R}^{n \times d_q}$ , keys  $\mathbf{K} \in \mathbb{R}^{n \times d_k}$ , values  $\mathbf{V} \in \mathbb{R}^{n \times d_v}$ , where  $\mathbf{Q} = \mathbf{X}\mathbf{W}_Q$ ,  $\mathbf{K} = \mathbf{X}\mathbf{W}_K$ ,  $\mathbf{V} = \mathbf{X}\mathbf{W}_V$ , and  $d, d_q, d_k, d_v$  are the dimensions of inputs, queries, keys and values ( $d_k = d_q$ ), respectively. The output of the self-attention layers is,

$$\text{attention}(\mathbf{Q}, \mathbf{K}, \mathbf{V}) = \text{softmax} \left( \frac{\mathbf{Q}\mathbf{K}^T}{\sqrt{d_q}} \right) \mathbf{V}. \quad (2)$$

Afterward, the output of the  $H$  different self-attention layers is then concatenated and linearly transformed to multi-head attention output,  $\text{MultiHeadAttnOutput} = \text{Concat}(\text{head}_1, \dots, \text{head}_H)\mathbf{W}_Z$ , where  $\text{head}_i = \text{attention}(\mathbf{Q}_i, \mathbf{K}_i, \mathbf{V}_i)$ ,  $\mathbf{W}_Z \in \mathbb{R}^{H \cdot d_v \times d}$ . Besides, a residual connection module followed by a layer normalization module is inserted around each module. That is,  $\mathbf{H}' = \text{LayerNorm}(\text{Attn}(\mathbf{X}) + \mathbf{X})$ ,  $\mathbf{H} = \text{LayerNorm}(\text{FFN}(\mathbf{H}') + \mathbf{H}')$ , where  $\text{Attn}(\cdot)$  denotes multi-head attention module,  $\text{LayerNorm}(\cdot)$  denotes the layer normalization operation, and  $\text{FFN}(\cdot)$  denotes the feed-forward network as  $\text{FFN}(\mathbf{H}') = \text{ReLU}(\mathbf{H}'\mathbf{W}_1 + \mathbf{b}_1)\mathbf{W}_2 + \mathbf{b}_2$ , where  $\mathbf{W}_1, \mathbf{W}_2, \mathbf{b}_1, \mathbf{b}_2$  are trainable parameters.

In recent years, the development of large language models (LLMs) based on the transformer has been driven by the availability of massive amounts of data and the increasing computational power. Based on the transformer architecture, LLMs, often with hundreds or even trillions of parameters, have achieved remarkable performance on a wide range of tasks, such as language processing and planning, scientific discovery<sup>84-87</sup>. Typically, LLMs undergo a pre-training phase on vast corpora of text data, which enables them to discern and assimilate prevalent linguistic patterns. Subsequent fine-tuning on task-specific datasets further refines their performance and adaptability. Some notable examples of large language models include BERT<sup>88</sup>, OPT<sup>89</sup>, GPT<sup>90</sup>, Llama<sup>91</sup>, etc. Recently, the surge in multimodal data generation within scientific domains, such as molecular structures, proteins, and genomes, has catalyzed the development of scientific LLMs designed to comprehend, interpret, and generate specialized scientific languages<sup>87</sup>. These scientific LLMs include medical LLMs<sup>92,93</sup>, biological LLMs<sup>94-96</sup>, chemical LLMs<sup>97-99</sup>, and comprehensive LLMs<sup>100,101</sup>.

### 3.4 Diffusion Models

Deep generative models have emerged as a transformative force in deep learning, enabling the generated data samples to resemble the real data<sup>102-106</sup>. Traditional generative models such as Variational Autoencoders (VAE)<sup>107,108</sup> and Generative Adversarial Networks (GANs)<sup>109</sup> have significantly advanced data generation tasks. VAEs encode input data into latent variables and then decode the latent variables back to new samples. GANs, on the other hand, use an adversarial framework of two neural networks: a generator to synthesize data and a discriminator to distinguish whether samples are real or fake. However, these models often suffer from low-fidelity generative samples, mode collapse, or training instability<sup>110</sup>.

Recently, diffusion models have exhibited advantages over traditional generative models by providing higher fidelity samples. Diffusion models generate data by gradually adding noise, namely the forward diffusion process, and reconstructing data by progressively removing the noise, namely the reverse diffusion process<sup>111,112,112,113</sup>. Specifically, the forward process incrementally adds noise to the real data  $\mathbf{x}_0 \sim q(\mathbf{x}_0)$  over  $T$  timesteps,

$$q(\mathbf{x}_{1:T}|\mathbf{x}_0) = \prod_{t=1}^T q(\mathbf{x}_t|\mathbf{x}_{t-1}), \quad q(\mathbf{x}_t|\mathbf{x}_{t-1}) = \mathcal{N}(\mathbf{x}_t; \sqrt{1 - \beta_t}\mathbf{x}_{t-1}, \beta_t\mathbf{I}). \quad (3)$$

This phase is mathematically represented as a sequence of states, each representing a progressively noisier state compared to the preceding states. Conversely, the reverse diffusion process learns to reconstruct the original data  $p_\theta(\mathbf{x}_0)$  by progressively removing the noise.

$$p_\theta(\mathbf{x}_{0:T}) = p(\mathbf{x}_T) \prod_{t=1}^T p_\theta(\mathbf{x}_{t-1}|\mathbf{x}_t), \quad p_\theta(\mathbf{x}_{t-1}|\mathbf{x}_t) = \mathcal{N}(\mathbf{x}_{t-1}; \mu_\theta(\mathbf{x}_t, t), \Sigma_\theta(\mathbf{x}_t, t)). \quad (4)$$

The reverse diffusion process uses a neural network  $\mu_\theta$  to recover the denoised state from the noisy input. Through the forward and reverse diffusion process, new data samples can be generated.

## 4 Material Discovery Tasks

### 4.1 Physicochemical Property Prediction

Identifying crystalline materials properties is a complex task that involves theoretical and experimental methods. Classical *ab initio* physical simulation techniques, such as DFT<sup>134</sup>, can precisely calculate material properties, including electronic structures, phonon spectra, and tensor properties. However, these methods are computationally intensive, which limits their practical

**Table 1.** The Summary of Models for Material Property Prediction

Methods	Data representations	Fundamental models	Physical knowledge	The predicted properties
SchNet <sup>24,114</sup>	Geometric graph	GGNN	-	Formation energy, band gap, etc
CGCNN <sup>23</sup>	Geometric graph	GGNN	-	Total energy, band gap, etc
MEGNET <sup>25</sup>	Geometric graph	GGNN	Global state, e.g. temperature	Formation energy, band gap, etc
GATGNN <sup>115</sup>	Geometric graph	GGNN	-	Formation energy, band gap, etc
ALIGNN <sup>116,117</sup>	Geometric graph	GGNN	-	Electron DOS, band gap, etc
ECN <sup>118</sup>	Geometric graph	GGNN	Space group	Formation energy, band gap, etc
PotNet <sup>119</sup>	Geometric graph	GGNN	Interatomic potentials	Total energy, band gap, etc
CrysGNN <sup>120</sup>	Geometric graph	GGNN	-	Total energy, band gap, etc
ETGNN <sup>121</sup>	Geometric graph	GGNN	-	Dielectric, piezoelectric, and elastic tensors
DTNet <sup>122</sup>	Geometric graph	GGNN	-	Dielectric tensor
GMTNet <sup>123</sup>	Geometric graph	GGNN	Space group	Dielectric, piezoelectric, and elastic tensors
CEGANN <sup>124</sup>	Geometric graph	GGNN	-	Grain boundary, etc
ComFormer <sup>125</sup>	Geometric graph	Transformer	-	Total energy, band gap, etc
Crystalformer (ICLR) <sup>126</sup>	Geometric graph	Transformer	Interatomic potentials	Total energy, band gap, etc
Crystalformer (AAAI) <sup>127</sup>	Geometric graph	Transformer	-	Total energy, band gap, etc
E(3)NN <sup>128</sup>	Geometric graph	GGNN	-	Phonon DOS, electron DOS, etc
DOSTransformer <sup>129</sup>	Geometric graph	Transformer	Energy level of material	Phonon DOS, electron DOS, etc
Matformer <sup>130</sup>	Geometric graph	Transformer	-	Total energy, band gap, etc
CrysDiff <sup>131</sup>	Geometric graph	Diffusion + GGNN	Space group	Total energy, band gap, etc
MOFTransformer <sup>132</sup>	Geometric graph	Transformer	-	Adsorption properties, band gap, etc
Uni-MOF <sup>5</sup>	Geometric graph	Transformer	Global state, e.g. temperature	Adsorption properties
SODNet <sup>133</sup>	Geometric graph	Transformer	Disordered structure of superconductors	Critical temperature of superconductors

applicability. Recently, deep learning techniques offer an efficient way for material properties predictions<sup>119,125,126,129–131,135</sup>. These deep neural networks aim to capture the mapping relationship between crystalline materials data and properties from the collected datasets. Current related works can be categorized into GNN-based methods and transformer-based methods. Based on this taxonomy, Table 1 provides a summary of the used data representations, fundamental models, and the predicted properties.

#### 4.1.1 Geometric Graph Neural Network-Based Prediction

Due to the inherently periodic and the infinite arrangement of lattice within 3D Euclidean space, GGNN-based property prediction methods necessitate graph construction techniques to effectively represent the infinite lattice and its atomic interactions. Typically, nodes in the graph correspond to atoms and their periodic replicas across the crystal’s 3D structure, while edges represent the interactions between these atoms. Following the graph construction, GGNN-based methods employ supervised learning to train the network on a dataset of crystal properties. Once trained, the GGNN is leveraged to predict the properties of crystalline materials.

An exemplary application of GGNNs is SchNet<sup>24,114</sup>, which was initially designed for simulating quantum interactions in molecules using continuous-filter convolutional layers. This method directly models interactions between atoms utilizing distance information, thereby providing rotation invariant energy predictions. Although SchNet can effectively handle local environments, it may fall short in capturing more complex long-range interactions and global geometric structures. Compared to SchNet, CGCNN<sup>23</sup> is a pioneering GGNN specifically designed for handling crystal structures and it can extract both local and global features. This model was the first to represent crystal structures as multi-edge graphs, as shown in FIG. 3a. In the multi-edge graph, nodes represent atoms and all their copies within the 3D space, while edges represent the connections between these atoms. The multi-edge connections between nodes reflect the periodicity of the crystal, connecting atoms from different unit cells. Once the crystal graph is constructed, CGCNN uses convolution and pooling layers to extract and learn both local and global features of the structure. Furthermore, by separating the convolution and pooling layers, CGCNN is capable of learning the contributions of different local chemical environments to the target properties, thus providing interpretable predictions of material properties. As depicted in FIG. 3a, the bottom left shows a line chart of MAE loss using different graph convolution functions, and the bottom right is a 2D histogram representing the predicted formation energy per atom against the DFT calculated value. CGCNN has achieved good results. Despite the impressive results, there remains significant potential for further advancements. For instance, CGCNN lacks the capability to account for global state variables (such as

temperature), which are essential for predicting state-dependent properties (such as free energy). Additionally, though CGCNN has demonstrated remarkable potential in learning flexible global feature representations, they often underperform in capturing local environments compared to their predictability for global properties like energy band gaps.

Correspondingly, the MEGNet model<sup>25</sup> addresses the first limitation by incorporating global state inputs, including temperature, pressure, and entropy. In MEGNet, the embeddings of global state information are updated simultaneously during the updates of bond and node embeddings. CEGANN<sup>124</sup> advances the classification potential of GGNNs at both the structural (global) and atomic (local) levels simultaneously. This multi-scale classification method, based on a graph attention architecture, enables the classification of features from atomic-scale crystals to heterogeneous interfaces and micro-scale grain boundaries. As demonstrated in FIG. 3b, CEGANN begins by constructing an edge graph of the crystal based on the crystal graph. The edge and angle feature representation of the crystal structure is then processed through hierarchical message-passing blocks, generating feature representations for each structure to be used in prediction tasks. This robust approach can be applied to tasks such as the space group classification of crystals (as shown in FIG. 3b), grain boundary recognition, and the analysis of other heterogeneous interfaces.

GATGNN<sup>115</sup> enhances CGCNN by integrating augmented graph attention layers and global attention layers, thereby leveraging the varying contributions of different atoms in a crystal to the overall material properties. The augmented graph attention layer aggregates information from neighboring nodes by calculating attention weights between them, whereas the global attention layer processes the graph's overall structure. However, GATGNN also has some drawbacks. For example, the application of the softmax function imposes constraints on the ability of GATGNN to distinguish nodes with different degrees. Contrasting with traditional GGNN architectures like CGCNN, MEGNet, and GATGNN, ALIGNN employs a line graph neural network derived from the crystal graph<sup>116,117</sup>. This derived graph describes the connectivity of the edges in the original crystal graph, with its nodes corresponding to atomic bonds and its edges representing bond angles. ALIGNN alternates message passing on these two graphs, leveraging bond lengths and angles in the line graph to incorporate detailed atomic structural information, thus enhancing the model's performance. However, the more intricate graph construction methods employed by ALIGNN result in a heightened computational complexity.

Recent advancements in GGNN methodologies have increasingly focused on leveraging the intrinsic properties of crystalline materials. Compared to molecules, crystals typically exhibit higher structural symmetry – a property often overlooked by earlier models. Kaba *et al.*<sup>118</sup> addressed this by developing an equivariant model tailored to crystal space groups. CrysGNN<sup>120</sup> introduces a pre-training framework. During its pre-training phase, CrysGNN reconstructs node features and connectivity in a self-supervised manner. Additionally, it leverages space group and crystal system information to learn structural similarities between graph structures. This paradigm enables CrysGNN to utilize latent chemical and structural information embedded in large volumes of unlabeled crystal data, which can then be used to distill the property predictor, improving the accuracy of property prediction. The improvements range from 4.19% to 16.20%. PotNet<sup>119</sup> models interatomic potentials directly as edge features to capture interactions in infinite space. This edge feature implicitly encodes information about crystal periodicity, thereby enabling a fully connected GNN to be informed of crystal periodicity. To address the substantial computational demands of supervised learning approaches for crystal property prediction, Song *et al.*<sup>131</sup> introduced CrysDiff, a pretrain-finetune framework specifically designed for property prediction tasks. CrysDiff consists of two stages: pre-training and fine-tuning. In the pre-training stage, CrysDiff learns the latent marginal distribution of the crystal structures based on the diffusion model. During the fine-tuning stage, CrysDiff learns the distribution of crystal properties by training a multi-layer perception while keeping the input crystal structure unchanged. The pre-training stage enables CrysDiff to learn to recognize important patterns within crystal structures, which accelerates the learning process in the fine-tuning stage. Experimental results indicate that CrysDiff markedly enhances the performance of downstream crystal property prediction tasks across a range of target properties.

The previously mentioned GGNNs have primarily focused on predicting single-value properties of crystals. These methods cannot be directly applied to tensor property prediction as they fail to achieve  $O(3)$  equivariance for tensor property prediction. To address this challenge, Edge-based Tensor Prediction Graph Neural Network (ETGNN)<sup>121</sup> represents a crystal's tensor properties as the average tensor contributions from all atoms in the crystal. Each atom's tensor contribution is expressed as a linear combination of local spatial components projected onto the directions of edges in multiple-sized clusters. This tensor decomposition is rotationally equivariant, making ETGNN applicable to tensor property prediction. Dielectric Tensor Neural Network (DTNet)<sup>122</sup> employs a strategy similar to ETGNN, utilizing tensor products to ensure the transfer of tensor equivariance. However, DTNet distinguishes itself by applying tensor products to the equivariant features generated in the network's output, rather than directly on the edge features of the crystal graph. Furthermore, in its experimental evaluation, DTNet was applied to screen the Materials Project dataset, effectively identifying potentially stable materials with high dielectric constants.

Although ETGNN and DTNet achieved good performance, they failed to enforce crystal symmetry constraints in tensor predictions. As an alternative method designed to predict general tensor properties of crystalline materials, GMTNet<sup>123</sup> has made improvements in crystal symmetry constraints. Within the broader GGNN framework, GMTNet adopts the transformer

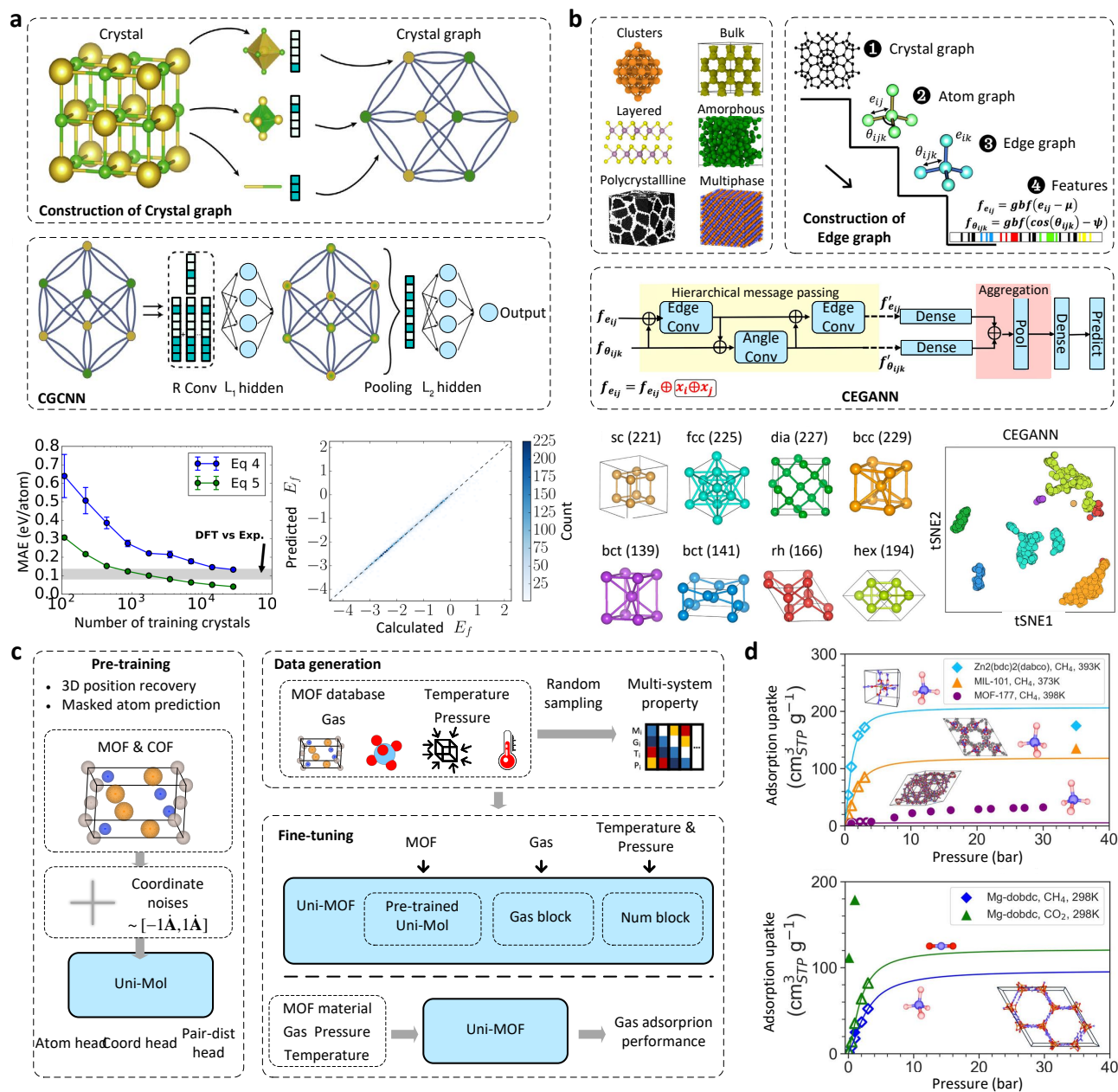


**Figure 3. GGNN-based and transformer-based methods for property prediction.** **a** | Schematic of CGCNN method. This model first represents crystal structures as multi-edge graphs and then uses graph convolutional neural networks to extract information accordingly. CGCNN experimental results (bottom): The left side shows a line chart of MAE loss using different graph convolution functions, and the right side is a 2D histogram representing the predicted formation energy per atom against the DFT calculated value. **b** | CEGANN begins by constructing an edge graph of the crystal based on the crystal graph. The edge and angle feature representation of the crystal structure is then processed through hierarchical message-passing blocks, generating feature representations for each structure to be used in prediction tasks. The bottom shows the classification experiment results. **c** | Schematic of Uni-MOF. In the pre-training phase, in addition to predicting the types of occluded atoms, a 3D position denoising task is used to learn 3D spatial representations. Cross-system performance datasets can be collected or randomly sampled under different operating conditions. During the fine-tuning phase, a unified gas adsorption prediction model, Uni-MOF, is established by embedding pre-trained weights, MOF materials, gas, temperature, and pressure. **d** | Uni-MOF experimental results: adsorption isotherms based on low-pressure predictions and high-pressure experimental values. Panel **a** is adapted from REF.<sup>23</sup>. Panel **b** is adapted from REF.<sup>124</sup>. Panel **c** and **d** adapted from REF.<sup>5</sup>.

strategy from ComFormer<sup>125</sup> to update node-invariant features. It employs spherical harmonic filters and tensor product convolutions to achieve equivariant message passing, updating edge features. Additionally, GMTNet incorporates a crystal symmetry enforcement module that simplifies complex symmetry constraints of tensor properties into constraints applicable to crystal-level features. This architecture enhances the network's robustness against minor errors in message-passing operations and crystal inputs.

#### 4.1.2 Transformer-Based Prediction

Recently, transformer-based architectures have shown remarkable capability in graph learning<sup>136</sup>, and recent works have attempted to apply these architectures to material property prediction. One representative is Matformer<sup>130</sup>, which leverages the geometric distances between atoms from two adjacent unit cells to encode periodic patterns. This enables Matformer to effectively encapsulate the lattice information and periodic patterns. However, Matformer occasionally encodes crystals of different structures as identical graphs<sup>125</sup>. To address this issue, ComFormer<sup>125</sup> proposed SE(3) invariant graph representation and SO(3) equivariant graph representation to capture the local and global geometric information by leveraging atomic interatomic distances and atomic angle information. Then, ComFormer converts the two types of graph representations into embeddings by using transformers, including the node-wise transformer layer and edge-wise transformer layer. This enables ComFormer to delicately capture geometric information of different structures.

On the other hand, Matformer only encodes atomic distance as edge features. To enrich the edge features' expressiveness, CrystalFormer<sup>127</sup> incorporates angular information into the edge features. In addition, CrystalFormer introduces a graph construction method specifically designed for periodic invariance, using different penalty weights to select appropriate atomic neighborhoods to model the local atomic environments. To further broaden the use of transformer in property prediction, DOSTransformer<sup>129</sup> is specifically designed for the prediction of the density of states (DOS), which is a task not addressed by Matformer. Since DOS is influenced not only by the material itself but also by the energy levels, DOSTransformer takes both the crystal material and energy as heterogeneous input modalities.

Metal-organic frameworks (MOFs) are a class of crystalline porous materials formed through the self-assembly of metal ions or metal clusters with organic ligands via coordination bonds. Due to their unique porous structure, they have garnered much attention in areas such as gas storage and catalysis. MOFTransformer<sup>132</sup> focuses on MOFs' various properties prediction, including gas adsorption and electronic properties. This work is first pre-trained on extensive MOFs, where graph embedding and energy grid embedding are regarded as multi-modal information to enhance generalizability. Then, the MOFTransformer can be fine-tuned for various properties prediction tasks, e.g., gas adsorption uptake prediction.

MOFTransformer can only predict the adsorption uptake under certain external conditions, which limits the model's generalizability. To make predictions across various external conditions, Uni-MOF<sup>5</sup> is pre-trained on extensive datasets comprising MOFs and covalent organic frameworks (COFs) and subsequently fine-tuned to predict adsorption properties under various conditions such as gas molecules, temperature, and pressure (see FIG. 3c). During pre-training, Uni-MOF performs masked atom prediction and introduces noise into the original coordinates of MOFs. This strategy promotes its robustness and generalization capabilities. The fine-tuning stage trains the model under various adsorption conditions, enabling the fine-tuned Uni-MOF to predict adsorption properties under a range of conditions, including different gases, temperatures, and pressures. As shown in FIG. 3d, Uni-MOF successfully predicted the gas adsorption isotherms of different MOF structures at various temperatures.

## 4.2 Crystalline Material Synthesis

Traditionally, materials discovery heavily relied on intuition, trial-and-error experimentation, and serendipity. However, the chemical space of crystalline structures is immense, making it infeasible to explore new materials through traditional approaches. In recent years, deep generative models such as GANs, VAEs, diffusion, flow matching, transformer, etc, have offered a promising avenue for accelerating crystalline material discovery<sup>9, 27, 137-140</sup>. According to data representation, these methods fall into two categories: geometric graph-based generation and string-based generation. Based on this taxonomy, Table 2 provides a brief summary of the used data representations, fundamental models, and used physical knowledge.

### 4.2.1 Geometric Graph-Based Generation

Due to the bedrock of GGNNs in modeling geometry, a considerable amount of studies use GGNNs to model and generate crystalline materials<sup>147, 160-163</sup>. One pioneer is G-SchNet<sup>141</sup>. G-SchNet incorporates the constraints of Euclidean space and the rotational invariances of the atom distribution as prior knowledge. By using the distance between the previously placed positions and the next atomic position as constraints, an equivariant conditional probability distribution is constructed to determine the next atomic position. However, G-SchNet was originally proposed for small molecules, and it falls short of leveraging lattice information to model crystalline materials.

One representative work specifically designed for crystalline materials is CDVAE<sup>9</sup>. By using the SE(3) invariant GGNN as the encoder, CDVAE explicitly encodes the geometry graph and its lattice as invariant variables. Conditioning on these

**Table 2.** Summary of Deep Generative Models for Material Generation

Methods	Data representations	Fundamental models	Physical knowledge/constraints
G-SchNet <sup>141</sup>	Geometric graph: Cartesian sys.	GGNN	Non-bonded interaction and local symmetry
CDVAE <sup>9</sup>	Geometric graph: Cartesian sys.	VAE + Diffusion + GGNN	Harmonic force field approximation
Con-CDVAE <sup>142</sup>	Geometric graph: Cartesian sys.	VAE + Diffusion + GGNN	Same as CDVAE; property constraints
Cond-CDVAE <sup>143</sup>	Geometric graph: Cartesian sys.	Diffusion	Same as CDVAE; property constraints
LCOMs <sup>144</sup>	Geometric graph: Cartesian sys.	Diffusion	Same as CDVAE; property constraints
DiffCSP <sup>137</sup>	Geometric graph: fractional sys.	Diffusion + GGNN	Periodic equivariance
DiffCSP-SC <sup>133</sup>	Geometric graph: fractional sys.	Diffusion + GGNN	Periodic equivariance
EquiCSP <sup>145</sup>	Geometric graph: fractional sys.	Diffusion + GGNN	Lattice equivariance
GemsDiff <sup>146</sup>	Geometric graph: Cartesian sys.	Diffusion + GGNN	Composition constraint
SyMat <sup>8</sup>	Geometric graph: Cartesian sys.	VAE + Diffusion + GGNN	Permutation and rotation invariance
EMPNN <sup>147</sup>	Geometric graph: Cartesian sys.	GGNN	Lattice equivariance
UniMat <sup>148</sup>	Geometric graph: Cartesian sys.	Diffusion	-
MatterGen <sup>26</sup>	Geometric graph: fractional sys.	Diffusion + GGNN	-
PGCGM <sup>139</sup>	Geometric graph: fractional sys.	GAN	Atomic distance constraint; symmetry constraint
CubicGAN <sup>149</sup>	Geometric graph: fractional sys.	GAN	Symmetry constraint
PCVAE <sup>150</sup>	Geometric graph: Cartesian sys.	VAE	Lattice and symmetry constraint
DiffCSP++ <sup>60</sup>	Geometric graph: fractional sys.	Diffusion + GGNN	Symmetry constraint using Wyckoff position
FlowMM <sup>140</sup>	Geometric graph: fractional sys.	Flow matching + GGNN	Symmetry constraint
Govindarajan <sup>151, 152</sup>	Geometric graph: Cartesian sys.	GGNN	-
CHGFlowNet <sup>153</sup>	Geometric graph: Cartesian sys.	GGNN	Symmetry constraint
LM-CM,LM-AC <sup>154</sup>	String: CIFs	LLM	-
CrystaLLM <sup>155</sup>	String: CIFs	LLM	-
CrystalFormer <sup>27</sup>	String: CIFs	Transformer	Symmetry constraint using Wyckoff position
SLI2Cry <sup>44</sup>	String: SLICES	RNN	-
Gruver <sup>53</sup>	String: CIFs	LLM	-
FlowLLM <sup>156</sup>	Geometric graph: Cartesian sys.	LLM + Flow matching	-
Mat2Seq <sup>157</sup>	String	LLM	Symmetry constraint
GenMS <sup>158</sup>	String: CIFs	LLM + Diffusion	Property constraints
ChemReasoner <sup>159</sup>	String	LLM + GGNN	Property constraints

invariant variables, CDVAE generates materials in a diffusion process that moves atomic coordinates towards a lower energy state and updates atom types to satisfy bonding preferences between neighbors. CDVAE shows nearly 100% structure validity and composition validity when using the Perov-5 dataset<sup>164</sup> and the MP-20 dataset<sup>9</sup>. In particular, CDVAE employs a property predictor to guide the diffusion model to generate materials with specific properties. To achieve the goal, CDVAE applies gradient ascent to optimize those invariant variables and uses the property predictor to predict the property of the corresponding generated materials. After optimizing, 90% generated materials are in the top 15% of the energy distribution in the MP-20 dataset.

Based on the CDVEA, researchers have made several extensions. Towards generating stable crystal structure, LCOMs<sup>144</sup> expands on CDVAE to locate the structures with the lowest energy by using gradient-based optimization techniques to the latent variables. After optimizing latent variables, the energy improvement can be up to 5% on the MatBench dataset<sup>165</sup>. Cond-CDVEA<sup>143</sup> integrates the DimeNet++<sup>166</sup> as the encoder and GemNet-dQ<sup>167</sup> as the decoder for conditional generation, making it be capable of generating diverse crystal structures conditioned on various chemical composition and pressure. In particular, it can accurately predict 59.3% of the 3,547 unseen ambient-pressure experimental structures within 800 structure samplings, with the accuracy rate climbing to 83.2% for structures comprising fewer than 20 atoms per unit cell. Con-CDVEA<sup>142</sup> generates crystals' latent variables according to given properties (e.g., formation energy, band gap, crystal system, combination of formation energy and band gap) and then yields the corresponding crystal structure by decoding the latent variables.

Early works often used Cartesian coordinate systems to represent and model geometric graphs. Recently, a number of

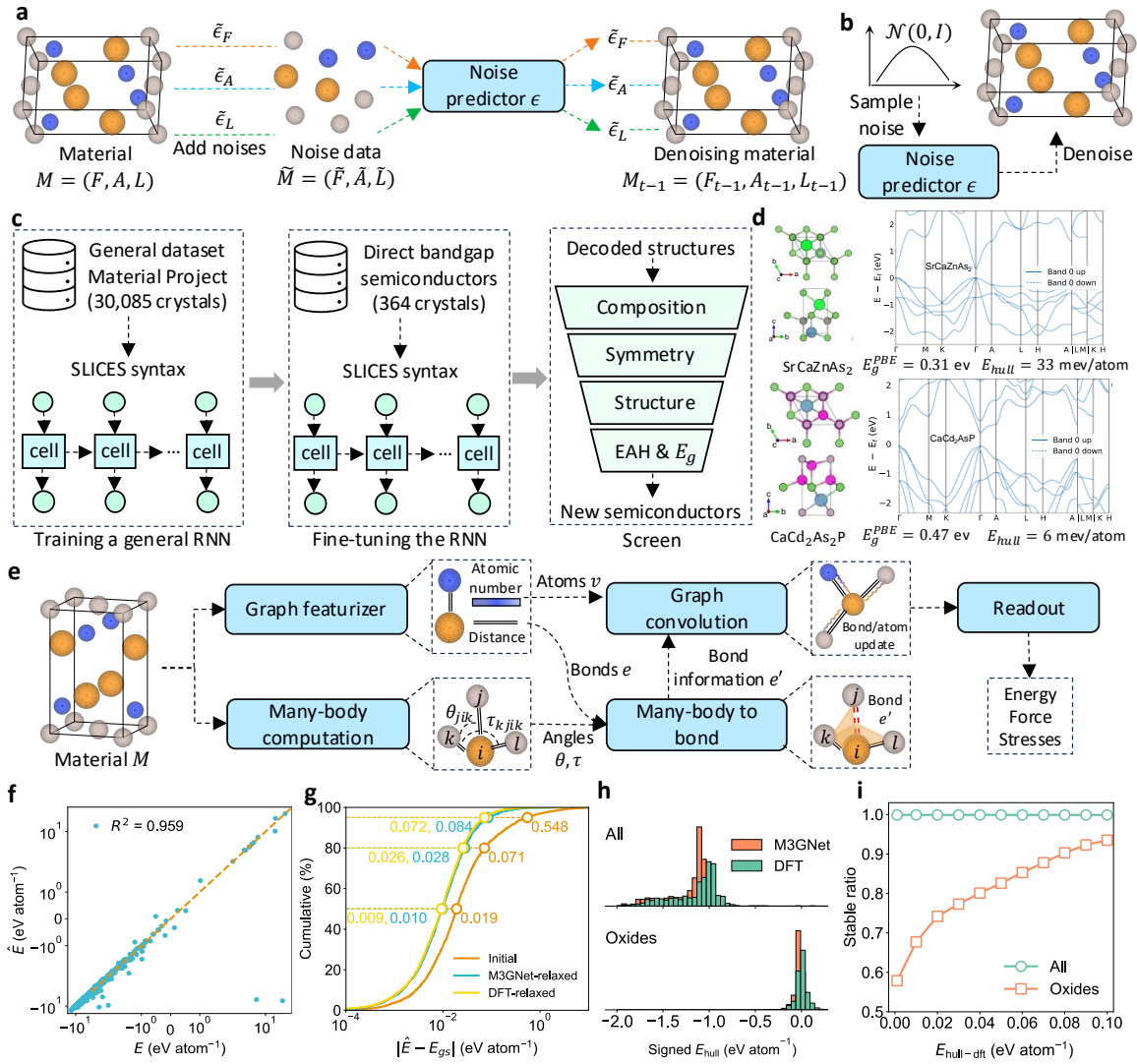


**Figure 4. GGNN-based and string-based methods for materials generation.** **a** | For the training stage, DiffCSP adds noises and denoises for atoms, factorial coordinates, and lattice parameters. **b** | For the generation stage, random noises are sampled from Gaussian space for denoising as new materials. **c** | Schematic overview of SLI2Cry. The data from Materials Project are converted to SLICES strings and then used to train a general RNN. The RNN is then fine-tuned on a direct bandgap semiconductors dataset. A great number of SLICES strings are sampled from the RNN and decoded. By filtering composition, symmetry, structure, and EAH &  $E_g$ , new direct narrow-gap semiconductors can be identified. **d** | The generated materials with their PBE band structures, the values of bandgap at the PBE level ( $E_g^{PBE}$ ), and energy above hull ( $E_{hull}$ ). **e** | M3GNet mainly includes five blocks: graph featurizer, many-body computation, graph convolution, many-body to bond, and readout. The graph featurizer extracts the atom and bond distance information. Many-body computation calculates the angles  $\theta$  and  $\tau$  between three bodies and many bodies, respectively. Many-body to bond calculates the new bond information by considering the full bonding environment via angles  $\theta$ ,  $\tau$ , and bond distance. The standard graph convolution updates bond and atom information, iteratively. The readout stage is an MLP to obtain the final embedding for predicting energy, force, and stresses. **f** |  $R^2$  values for the linear fitting between DFT and the predicted energy. **g** | The differences between M3GNet-predicted energies  $\hat{E}$  and ground state energies  $E_{gs}$  using the initial, M3GNet-relaxed, and DFT-relaxed structures.  $E_{gs}$  is defined as the DFT energy of the DFT-relaxed crystal. The horizontal lines mark the 50th, 80th, and 95th percentiles of the distributions, and the corresponding x-axis values are annotated. **h** | The signed  $E_{hull}$  distribution for the top-1000 lowest  $E_{hull-m}$  materials from any chemistry (All) and oxides only (Oxides). **i** | Fraction of materials below  $E_{hull-dft}$  among top-1000 materials in the All and Oxides categories. Panels **a** and **b** adapted from REF.<sup>60</sup>. Panels **c** and **d** adapted from REF.<sup>44</sup>. Panels **e**~**i** adapted from REF.<sup>41</sup>.

studies have used the fractional coordinate system instead of Cartesian coordinate systems to better reflect the symmetry of the underlying lattice. DiffCSP<sup>168</sup> utilizes the fractional coordinate system to intrinsically represent crystals and model periodicity. In particular, by employing an equivariant graph neural network for the denoising process, DiffCSP<sup>168</sup> introduced an equivariant diffusion approach, which conducts joint diffusion on lattices and fractional coordinates to comprehensively capture the crystal geometry, thereby enhancing the modeling of the crystal geometry. As shown in FIG. 4a, DiffCSP separately and simultaneously adds noise process and denoises on the fractional coordinates  $F$ , atom types  $A$ , and lattices  $L$ . For the generation stage, random noises are sampled from Gaussian space for denoising as new materials, as shown in FIG. 4b. DiffCSP achieves comparable validity with previous methods, e.g., CDVAE, but significantly outperforms previous methods in terms of the target properties. Following this, Chen *et al.*<sup>133</sup> extended DiffCSP for superconductor generation. In addition, EquiCSP<sup>145</sup> keeps lattice permutation equivariance in diffusion models by incorporating a permutation invariance penalty term during the denoising model training. EquiCSP maps all equivalent periodic data to the same representation and addresses periodic translation invariance. Compared to the DiffCSP method, EquiCSP fully realizes E(3) equivariance based on periodic graph symmetry during the diffusion training process.

Recently, several studies also sought to enhance the performance of generative models by integrating prior physical knowledge, such as introducing space group constraints directly into the model. Zhao *et al.* proposed a GAN model, called CubicGAN<sup>149</sup>, to generate large-scale cubic materials conditioning on the atom types and space groups. Further, Zhao *et al.*<sup>139</sup> also designed PGCGM, a physics-guided deep learning model for generating crystalline materials with high symmetry. Particularly, PGCGM devises two physics-oriented losses: atomic pairwise distance loss and structural symmetry loss, to ensure the structure validity. PGCGM increases the generation validity by more than 45% compared to CubicGAN. By using DFT calculations, 1869 out of 2000 generated materials were successfully optimized, of which 39.6% have negative formation energy, and 5.3% have energy-above-hull less than 0.25 eV/atom, indicating their thermodynamic stability and potential synthesizability. However, the application of PGCGM is constrained by ternary systems, thus limiting its universality.

Also, DiffCSP++<sup>169</sup> uses the diffusion model to generate new materials by incorporating the space group constraint. DiffCSP++ first encodes the lattice parameters as  $O(3)$ -invariant vector to ensure the lattice parameters satisfy the space group constraints. Then, DiffCSP++ generates only the atom associated with Wyckoff positions, thereby ensuring that the atom information within the unit cell satisfies the symmetry constrained by the space group. SyMat<sup>8</sup> aims to capture physical symmetries of periodic material structures, in which a score-based diffusion model generates atom coordinates and calculates coordinate matrix as scores to ensure symmetry. Compared to CDVAE, the rate of generated materials in the top 15% of energy distribution in the MP-20 dataset has increased by 7%.

To improve the generalizability across the periodic table, Zeni *et al.*<sup>26</sup> presented MatterGen, a model that generates stable, diverse inorganic materials across the periodic table. To enable this, MatterGen uses a diffusion model to produce crystalline structures by gradually refining atom types, coordinates, and the periodic lattice. In particular, an equivariant score network is pre-trained on a large dataset of stable material structures to jointly denoise atom types, coordinates, and the lattice. The score network is then fine-tuned with a labeled dataset, where the property labels are encoded to steer the generation towards a broad range of property constraints, such as desired chemistry, symmetry, and scalar property constraints. Compared to prior generative models such as CDVAE and G-SchNet, structures produced by MatterGen are more than twice as likely to be novel and stable, and more than 15 times closer to the local energy minimum.

Towards a generalized material representation, UniMat<sup>148</sup> defined a 4-dimensional material space that corresponds to the number of periods and groups in the periodic table, the maximum number of atoms per element in the periodic table, and the locations of each atom in a unit cell. The representation shows flexibility for smaller systems, as one can set the number of periods and groups in the periodic table to model specific chemical systems of interest. For example, set the number of periods and groups to 1 for modeling materials containing one specific element. With such a unified representation of materials, UniMat trains diffusion models by treating the representation as a 4-dimensional tensor input or condition. On Carbon-24, UniMat outperforms CDVAE in terms of property distribution, composition validity, and structure validity. On the more realistic MP-20 dataset, UniMat achieves the promising composition validity but worse structure validity than CDVAE.

In addition, a handful of works explore using reinforcement learning methods to autoregressively generate materials. Govindarajan<sup>151,152</sup> formulates the problem of designing new crystals as a sequential prediction task. At each step, given an incomplete graph of a crystal skeleton, an agent assigns an element to a specific node. The policy network is a graph neural network that transforms a given state into an effective representation and predicts the action. Similarly, CHGFlowNet<sup>153</sup> used a graph neural network-based hierarchical policy network to generate materials, where high-level decision-making policy operates on the space groups, and the low-level execution policy operates on the atom-lattices policy actions. These reinforcement learning methods show comparable performance and provide a new avenue for the exploration of chemical space.

#### 4.2.2 String-Based Generation

Crystalline materials are stored in standard text file formats known as CIFs. By treating CIFs as plain string representations, massive works explore the use of generative language models to generate crystals. The recently proposed invertible and

invariant crystal representation, SLICES, also provides a new avenue for using language models in material generation. In this part, we review these string-based generative models.

Several works simply use CIFs as inputs. Flam-Shepherd *et al.*<sup>154</sup> uses sequences of discrete tokens to represent everything in CIFs, such as atom coordinates and atom types. By encoding the data as tokens, it is simple to adapt LLMs to many different kinds of molecular structures, including small molecules, protein-binding pockets, and crystals. The work demonstrates that language models trained from scratch on many common molecular datasets actually outperform popular domain-specific models in their ability to generate valid compositions and structures. On the MP-20 dataset, LM-CM and LM-AC show nearly 90% structure validity and 90% composition validity. Also, Antunes *et al.*<sup>155</sup> developed a language model called CrystaLLM to generate crystal structures as discrete sequences by training from scratch on millions of CIF strings. Particularly, the integration with an energy predictor permits the use of a Monte Carlo tree search algorithm to search the structures with lower formation energy.

Cao *et al.*<sup>27</sup> introduced CrystalFormer, a transformer-based autoregressive model for space group-controlled crystalline materials generation. In CrystalFormer, the crystalline materials are represented by the Wyckoff letter, chemical elements, and fractional coordinates. To generate new samples, the transformer sequentially samples atom types, coordinates, Wyckoff positions, and lattice parameters. Compared to CDVAE, DiffCSP, and DiffCSP++, CrystalFormer can achieve comparable structure validity (approximately 100%) and composition validity (90%). Gruver *et al.*<sup>53</sup> showed that fine-tuned LLMs can generate the three-dimensional structure of stable crystals as text. The work converts the crystal lattice, atom identities, and atom positions into strings, and a LLM, LLaMA-2, is fine-tuned on the strings of inorganic materials. By using string formatted crystals and task-specific prompting, the work enables unconditional stable materials generation, text-condition materials generation, and structural infilling. By using DFT calculations, Gruver *et al.* showed that the fine-tuned LLaMA-2 can generate materials predicted to be metastable at about twice the rate (49% vs 28%) of CDVAE.

Due to the direct utilization of CIF files or similar text representations without a special process, these previously mentioned string-based generation methods often fail to ensure SE(3) invariance and periodic invariance within the model. To address this limitation, Mat2Seq<sup>157</sup> converts 3D crystal structures into 1D sequences through techniques such as Niggli cell reduction and irreducible atom sets. This approach ensures that varied mathematical descriptions of an identical crystal structure are consolidated into a single unique sequence, thereby achieving SE(3) and periodic invariance. Another way to ensure SE(3) invariance and periodic invariance is to generate string representation that satisfies both invertibility and invariances such as SLICES. SLI2Cry *et al.*<sup>44</sup> applies SLICES for the inverse design of direct narrow-gap semiconductors for optoelectronic applications. The schematic overview of SLI2Cry is given in FIG. 4c. Firstly, a general recurrent neural network (RNN) is trained on the Materials Project database to learn the syntax of SLICES strings and fine-tuned on a dataset of direct narrow-gap semiconductors. The fine-tuned RNN was used to generate large volumes of SLICES strings. Then, a great number of SLICES strings are sampled from the RNN and decoded into crystal structures. By filtering composition, symmetry, structure, and energy above hull (EAH) and  $E_g$ , 14 new direct narrow-gap semiconductors are identified. In FIG. 4d, examples of new materials and their Perdew-Burke-Ernzerhof (PBE) band structures are provided.

Beyond the direct use of LLMs to generate crystal representations, recent approaches have explored integrating LLMs with other generative techniques to enhance model performance in crystal structure generation. For example, FlowLLM<sup>156</sup> combines LLMs with Riemann Flow Matching (RFM) to improve generation fidelity. In this approach, the LLM is first fine-tuned to learn the data distribution of metastable crystals, enabling it to generate text representations of these structures. These string representations are then converted into geometric graph representations, and then RFM iteratively refines the atom coordinates and lattice parameters to produce stable crystal structures. FlowLLM achieves a roughly 50% improvement in stable, unique, and novel generation rates compared to previous models.

Additionally, GenMS<sup>158</sup> integrates LLMs with diffusion models. Initially, GenMS utilizes the LLM to generate intermediate textual representations of the crystal, such as chemical formulas. This intermediate information is then input into a diffusion model to produce crystal structures. GenMS then incorporates a neural network to predict the properties of the generated crystals, allowing for effective screening and selection of desirable structures. ChemReasoner<sup>159</sup> is a LLM-driven heuristic search framework for catalyst discovery. This work frames catalyst discovery as a search problem, where an agent, e.g., GPT-4, is informed by computational chemistry feedback to search favorable catalysts. Specifically, catalysts identified in the intermediate search steps are evaluated structurally based on spatial orientation, reaction pathways, and stability. A scoring function, which considers adsorption energies and reaction energy barriers, directs the LLM to focus on energy-efficient and effective catalysts.

### 4.3 Accelerating Theoretical Computations

Theoretical computations serve as indispensable tools for understanding the behavior of molecules and materials at the atomic and molecular levels, aiding in calculating various physicochemical properties. In this part, we investigate two primary methods: quantum mechanics and empirical force fields<sup>170</sup>. Although these methods can accurately simulate atomic systems,

both approaches encounter significant limitations — they are still challenged in complex atomic systems due to the massive computational demands. In this section, we present the recently proposed machine learning-assisted force field development and quantum mechanics for accelerating theoretical computations.

### 4.3.1 Force Field Development

Force fields or interatomic potentials are empirical models that use potential energy functions and parameters to describe the atomic interactions and dynamics for atomistic simulations. By learning accurate force fields, researchers can precisely model the behavior of materials at the atomic scale, thus understanding the property-structure relationships. Empirical force fields often rely on hand-crafted parameters, which are efficient yet inaccurate. On the other hand, the estimation of energy functions and parameters can be obtained by extensive optimization to fit the data from quantum mechanical calculations. They are accurate but inefficient. To strike a balance between accuracy and efficiency, machine learning-based force field methods have been proposed to model the force fields from calculation and experiment data.

The pioneer works of machine learning-based interatomic potentials leveraged descriptor-based frameworks with shallow neural networks or Gaussian Processes<sup>40,42,43</sup>. Behler *et al.*<sup>40</sup> proposed the first neural network potential, BPNN. In BPNN, an atomic descriptor (i.e., basis functions that transform an atomic configuration into a fixed-length fingerprint vector) based on the bond lengths and bond angles is passed to an MLP. On top of this formulation, a Monte Carlo dropout technique can be applied to the MLP to equip the potential with the ability to quantify its predictive uncertainty. Based on BPNN, various variants have been developed for molecular systems, such as water, methane, and other organic molecules<sup>40,171,172</sup>.

Recently, GGNNs have emerged as powerful deep-learning techniques for interatomic potentials due to their superior ability to incorporate invariant/equivariant symmetry constraints and long-range interaction<sup>173</sup>. They eliminate the need for hand-crafted descriptors. Cormorant<sup>174</sup> uses an equivariant neural network for property prediction on small molecules. This method is demonstrated on the potential energies of small molecules but not on atomic forces or systems with periodic boundary conditions. PotNet<sup>119</sup> models interatomic potentials by including the Coulomb potential, London dispersion potential, and Pauli repulsion potential. PotNet employs a message-passing scheme that considers interatomic potentials as well as efficient approximations to capture the complete set of potentials among all atoms. PotNet outperforms other methods on all four tasks, including the prediction of formation energy, band gap, bulk moduli, and shear moduli with the mean absolute error of 0.0188, 0.204, 0.040, and 0.065, respectively, on the Materials Project dataset.

Most previous GGNN-based force fields are based on two-atom interactions, known as two-body information, which means they only rely on the states of two atoms, known as two-body interactions. This is not in line with the actual situation, i.e., multiple atoms interact with each other. To address this limitation, MACE<sup>160</sup>, an architecture combining equivariant message passing with the efficient many-body message, aims to capture four-body interactions. MACE shows that using four-body messages reduces the required number of message passing iterations to just two, resulting in a fast prediction, reaching state-of-the-art accuracy of energy and force prediction on the small molecule datasets. In addition, DimeNet<sup>175</sup> enhances the use of pairwise interactions in a single convolution by integrating angular and three-body terms. DimeNet achieves a mean absolute error of 0.035 kcal mol<sup>-1</sup> for energy, 0.07 kcal mol<sup>-1</sup> for energy, and 0.17 kcal mol<sup>-1</sup> Å<sup>-1</sup> for forces on the MD17 dataset<sup>176</sup>, surpassing the performance of alternative GGNN models.

Towards the generalizability across the periodic table, Chen *et al.* used more than 187,000 energies, 16,000,000 forces, and 1,600,000 stresses from relaxation structures to train a universal deep learning framework for interatomic potentials, called M3GNet<sup>41</sup>. As shown in FIG. 4e. Firstly, many-body computation calculates the bond angles  $\theta$  and  $\tau$  between three atoms and many atoms, respectively. Then, the many-body to bond module leverages the angles  $\theta$ ,  $\tau$ , and bond distance to construct bond information  $e'$ . Afterward, a standard graph convolution updates bond and atom information by using bond information  $e'$  and atom information  $v$ . This many-body interaction considers richer angle information for material modeling, improving the performance of force field modeling. As shown in FIG. 4f and FIG. 4g, the energy predicted by M3GNet is very close to the energy calculated by DFT. M3GNet showcases the potential to learn the interatomic potential of various materials across the periodic table. As shown in FIG. 4h, for any chemistry (All) and oxides only (Oxides), the predicted signed  $E_{hull}$  distribution by M3GNet is close to DFT calculation. The stable ratio of the top-1000 lowest  $E_{hull-m}$  materials from All and Oxides is reported in FIG. 4i.

Although machine learning-based force field development has achieved the balance between efficiency and accuracy, they heavily rely on the large-scale labeled training data from quantum mechanics calculations, e.g., DFT. This computationally expensive data collection process has become a bottleneck in developing force fields. To reduce the cost of DFT labeled samples, Shui *et al.*<sup>177</sup> proposed two strategies to achieve weakly supervised learning of neural network potentials by utilizing physical information in empirical force fields. The first strategy is to train a classifier to select the best possible empirical force field for unlabeled samples and use the energy value calculated from this force field as the label value for the unlabeled sample to achieve data augmentation. The second strategy is based on transfer learning, which first trains on a large dataset obtained through empirical force fields and then uses DFT-labeled samples for fine-tuning. The experiment shows that the first strategy can improve performance by 5%~51%, while the second strategy can improve performance by up to 55%.

With the same goal of improving the data efficiency, NequIP<sup>43</sup> uses relative position vectors instead of simple distances (scalars), which not only contain scalars but also features of high-order geometric tensors. This changes the features to be rotation invariant and allows rotation invariant filters to use angle information. It employs E(3)-equivariant convolutions for interactions of geometric tensors, resulting in state-of-the-art accuracy and data efficiency. NequIP is applied to a catalytic surface reaction of heterogeneous catalysis of formate dehydrogenation, and it can obtain mean absolute errors in the force components of 19.9 meV/Å, 71.3 meV/Å, 13.0 meV/Å, and 47.6 meV/Å, on the four elements C, O, H, and Cu, respectively, as well as an energy mean absolute error of 0.50 meV/atom, demonstrating that NequIP is able to accurately model the interatomic forces for this complex reactive system.

On the other hand, the ion's valence can engage in different bonding depending on the number of electrons and the environment. Therefore, incorporating the impact of valence on chemical bonds into neural network potentials is very important. Traditional neural network potentials treat the elemental label as the basic chemical identity, but different valence states of transition-metal ions behave differently from each other as different elements. To narrow the research gap, CHGNet<sup>173</sup> takes a crystal structure with unknown atomic charges as input and outputs the corresponding energy, forces, stress, and magnetic moments (magnoms). The charge-decorated structure can be inferred from the on-site magnoms and atomic orbital theory. CHGNet regularizes the node-wise features at the convolution layer to contain the information about magnoms. The regularized features carry rich information about both local ionic environments and charge distribution. Therefore, the atom features used to predict energy, force, and stress are charge-constrained by their charge-state information. As a result, CHGNet can provide charge-state information using only the nuclear positions and atomic identities as input, allowing the study of charge distribution in atomistic modeling. CHGNet is pre-trained using energies, forces, stresses, and magnetic moments obtained from the Materials Project Trajectory Dataset<sup>173</sup> to learn the orbital occupancy of electrons, thereby enhancing its ability to describe both atomic and electronic degrees of freedom. Its effectiveness has been demonstrated in solid-state materials, including charge-informed molecular dynamics in  $\text{Li}_x\text{MnO}_2$ , the finite temperature phase diagram for  $\text{Li}_x\text{FePO}_4$ , and lithium diffusion in garnet conductors.

Despite the progress made, the current evaluation criteria for machine learning force fields are limited to the prediction accuracy of force and energy. Fu *et al.*<sup>178</sup> selected a series of systems, including water, organic small molecules, peptides, and crystal materials, and designed a series of evaluation criteria to describe trajectory stability, demonstrating that some machine learning force fields with high accuracy currently cannot reproduce dynamics trajectories well. The work suggested that stability should become a new criterion for evaluating machine learning force fields.

### 4.3.2 Aiding Quantum Mechanics

Force field development heavily relies on empirical data and may struggle with accuracy in complex systems. On the other hand, rigorous quantum mechanical approaches, e.g., DFT, provide a more accurate description of electronic structure within molecules and materials systems and thus accurately predict their behavior and properties. While DFT excels in accuracy, it is computationally demanding, especially for large systems, which can limit its practical applications.

To improve the efficiency of DFT, the tight-binding model provides a more streamlined approach. Tight-binding model is based on the assumption that electrons are tightly bound to their respective atoms and only interact with their nearest neighbors<sup>179-181</sup>. By using this approximation, the tight-binding model significantly reduces the computational cost while maintaining a level of accuracy. Building upon tight-binding methods, Density Functional Tight Binding (DFTB) emerges as an advanced method that combines the advantages of DFT with the efficiency of tight binding<sup>182-184</sup>. DFTB utilizes parameterized interactions derived from DFT calculations, allowing it to capture essential chemical properties while accelerating the computational process. This makes DFTB particularly useful for studying larger systems, such as complex materials and biomolecular structures<sup>170, 179, 185, 186</sup>.

Recently, incorporating machine learning into DFTB has further advanced the field<sup>179, 185, 187</sup>. They mostly learn from a vast dataset obtained by quantum mechanical calculations to learn the mapping from structure to Hamiltonians which is a bedrock property in DFT calculations. Wang *et al.* developed machine learning-based algorithms to generate tight-binding Hamiltonians matrices from electronic eigenvalues<sup>179</sup>. However, this approach neglected atomic structure information, limiting its applicability to "unseen" structures. Recently, a deep learning-based tight-binding method, dubbed DeePTB, is proposed<sup>185</sup>. DeePTB constructs tight-binding Hamiltonians using gauge-invariant parameters and then maps these parameters from symmetry-preserving local environment descriptors to obtain the tight-binding Hamiltonian and its corresponding eigenvalues. After supervised learning from training structures with ab initio eigenvalues, DeePTB can directly predict accurate tight-binding Hamiltonians. On the group IV and group III-V materials, exceptional agreement of eigenvalues from DeePTB Hamiltonians and those from ab initio calculations can be achieved, with the coefficient of determination  $R^2 \approx 0.9999$ .

Despite the progress, it should be pointed out that these methods are still mostly based on data-driven inference instead of physical laws. The physical laws governed by quantum mechanics indeed determine the atomic interactions. To address the issue, Stohr *et al.* proposed a hybrid quantum mechanics/deep learning formalism, called the DFTB-NN<sub>rep</sub><sup>170</sup>. DFTB-NN<sub>rep</sub> uses DFTB in conjunction with a global deep neural network. Specifically, the repulsive energies and forces are obtained

via a neural network model based on reference data, while the electronic energies and properties are calculated by DFTB. DFTB-NN<sub>rep</sub> has demonstrated highly accurate predictions of energetic, structural, and vibrational properties for a vast range of organic molecules across their respective conformational spaces.

#### 4.4 Aiding Characterization

Aiding characterization techniques, including XRD, SEM, SPM, and TEM, aim to provide insights into the microstructure, composition, and defects within materials, thereby facilitating the correlation between microstructural characteristics and their properties. In this part, we outline image-based aiding characterization and spectra-based aiding characterization. A more comprehensive review regarding the two aiding characterization techniques can be found in REF.<sup>35</sup>.

The atomistic images obtained by microscopy techniques can unveil their structural characteristics from microstructure to macrostructure. These structural characteristics are intimately connected to the materials' functionality and performance. Therefore, with the atomistic images, a broad portfolio of image-based material characterization techniques has been proposed to identify structural characteristics. In what follows, we briefly introduce some representative works in this field.

Ziletti *et al.*<sup>33</sup> paved the way for this application by creating a large database of perfect crystal structures. In particular, by training on the database, the proposed ConvNet uses CNNs to classify the space group of each diffraction pattern. Image-based characterization techniques have also been used to generate predictions for every pixel in an image, providing detailed information about the size, position, orientation, and morphology of features. Azimi *et al.*<sup>78</sup> developed an ensemble of fully CNNs to accurately segment martensite, tempered martensite, bainite, and pearlite in SEM images of carbon steels, achieving a remarkable accuracy of 94%. The methodology represents an advancement in automating the segmentation of different phases in SEM images. Yang *et al.*<sup>34</sup> utilized the U-net architecture to attain high accuracy in detecting vacancies and dopants in scanning transmission electron microscopy images, achieving a model accuracy of up to 98%. To classify these atomic sites, they grounded their approach in experimental observations, categorizing the sites into five distinct types: tungsten, vanadium replacing tungsten, selenium with no vacancy, monovacancy of selenium, and divacancy of selenium.

When electromagnetic radiation hits materials, the interaction between the radiation and the substance can be measured by the wavelength or frequency of the radiation — spectra signals. The spectra data are commonly obtained by XRD spectra and Raman spectra<sup>35–37, 188</sup>. XRD spectra, represented as plots of X-ray intensity versus the angle between the incident and diffracted beams, provide quantitative information about crystal structures, such as the positions and intensities of diffraction peaks, which correspond to interplanar spacings and crystallite sizes. Raman spectra, obtained by measuring the frequency shift of scattered light, provide characteristic information about molecular vibrations and crystal structures. Raman spectra can identify the chemical composition and crystal structure of materials.

Park *et al.*<sup>189</sup> analyzed 150,000 XRD patterns and utilized CNN models to predict structural information from the simulated patterns. The CNN models achieved accuracies of 81.14%, 83.83%, and 94.99% for space-group, extinction-group, and crystal-system classifications, respectively. Abhiroop *et al.*<sup>190</sup> proposed a framework using CNNs and long short-term memory networks for the automatic identification of complex polymorph structures from their Raman spectra. This framework can accurately recognize TiO<sub>2</sub> with different polymorphs. Stein *et al.*<sup>191</sup> explored the mapping between material images and their corresponding spectra using a conditional variational encoder, employing neural network models as the backbone. The model can generate spectra directly from straightforward material images, enabling significantly faster material characterizations.

## 5 Benchmarking and Software Platforms

The availability of substantial volume datasets and platforms is the fuel in the field of AI-driven materials science. In this section, we introduce commonly utilized datasets and platforms in crystalline material research.

1. *The Materials Project*<sup>20</sup>: The Materials Project (MP) harnesses the power of supercomputers alongside state-of-the-art quantum mechanics theories and DFT to systematically compute the properties of a vast array of materials. At present, the MP dataset encompasses over 120,000 materials, each accompanied by a comprehensive specification of its crystal structure and key physical properties, including band gap, EAH, and more.
2. *JARVIS-DFT*<sup>15</sup>: The Joint Automated Repository for Various Integrated Simulations (JARVIS) offers an extensive computational dataset comprising thousands of crystalline materials. Established as a component of JARVIS, JARVIS-DFT was initiated in 2017, encompassing data for approximately 40,000 materials. This dataset includes around one million calculated properties, such as crystal space groups, bandgaps, and bulk moduli.
3. *OQMD*<sup>192, 193</sup>: The Open Quantum Materials Database (OQMD) is a repository of thermodynamic and structural properties of inorganic materials, derived from high-throughput DFT calculations. Presently, it encompasses over 800,000 crystal structures. Beyond facilitating crystal structure generation and the prediction of crystal material performance, OQMD has been instrumental in addressing a diverse array of material science challenges<sup>192</sup>.

4. *Perov-5*<sup>164</sup>: Perov-5 is a specialized dataset designed to facilitate research on perovskite crystalline materials. It encompasses a total of 18,928 distinct perovskite materials, all sharing a common perovskite crystal structure but exhibiting compositional diversity. The dataset incorporates 56 different elements, with each unit cell containing five atoms.
5. *Carbon-24*<sup>194</sup>: Carbon-24 is a specialized scientific dataset for the study of carbon materials, comprising over 10,000 distinct carbon structures that share the same elemental composition but exhibit varied structural configurations. Each entry in this dataset consists solely of carbon atoms, with unit cells containing between 6 and 24 atoms. Furthermore, Carbon-24 provides an array of data on the physical, chemical, and mechanical properties of each material, encompassing electronic performance, thermal stability, and mechanical strength.
6. *Crystallography Open Database*<sup>195</sup>: The Crystallography Open Database (COD) is a crystallography database that specializes in collecting and storing crystal structure information for inorganic compounds, small organic molecules, metal-organic compounds, and minerals. It includes specific details such as crystal structure parameters (unit cell parameters, cell volume, etc.) and space group information, allowing for the export of crystal information files in CIF format.
7. *Raman Open Database*<sup>36</sup>: The Raman Open Database (ROD) is an open database that specializes in collecting and storing Raman spectroscopy data. It contains a large amount of Raman spectral data for crystalline materials, including the chemical formulas of the materials and corresponding Raman spectral information such as excitation wavelengths and intensities.
8. *Inorganic Crystal Structure Database*<sup>196,197</sup>: The Inorganic Crystal Structure Database (ICSD) is the world's largest database of fully evaluated and published crystal structure data, containing experimentally determined inorganic crystal structures as well as theoretically reported inorganic structures from the literature. The database currently includes detailed information on approximately 300,000 crystal structures, including elements, metal oxides, salts, alloys, and minerals, with details such as unit cell parameters, space groups, atomic coordinates, and more.
9. *Open Catalyst Project*<sup>21</sup>: The goal of Open Catalyst Project is to help artificial intelligence to simulate and discover new catalysts for renewable energy storage, aiming to help combat climate change. Currently, the Open Catalyst Project includes datasets such as Open Catalyst 2020 (OC20) and Open Catalyst 2022 (OC22), which are used to train machine learning models. These datasets collectively contain 1.3 million DFT structural relaxations (the atomic positions within the structure have been optimized to find the configuration with the lowest energy) and results from over 260 million single-point evaluations. They cover a wide range of surfaces, and adsorbates (molecules containing nitrogen, carbon, and oxygen chemistries). Besides, these datasets are divided into training, validation, and test sets, and are used for common situations in catalysis: predicting the properties of a previously unseen adsorbate, searching for a previously unseen crystal structure or composition.
10. *Python Materials Genomics*<sup>198</sup>: Python Materials Genomics (Pymatgen) is a robust, open-source Python library for materials analysis. Pymatgen offer a range of modules for handling crystal structures, band structures, phase diagrams, and material properties. It supports a wide array of input and output formats, including VASP, ABINIT, CIF, and XYZ. Additionally, Pymatgen features powerful data visualization capabilities, enabling the generation of images such as crystal structure plots, band structure diagrams, and phase diagrams.
11. *MatBench*<sup>165</sup>: MatBench is a benchmark test suite in the field of crystalline materials, which can be used to evaluate and compare the property prediction performance of various machine learning models. The original datasets used in MatBench primarily come from multiple public databases in materials science, such as OQMD, MP, etc. Additional modifications are then enumerated to tailor the datasets for machine learning applications.
12. *M<sup>2</sup> Hub*<sup>199</sup>: M<sup>2</sup> Hub is a machine learning toolkit for materials discovery research that covers the entire workflow, including problem formulation, data downloading, data processing, machine learning method implementation, machine learning training and evaluation procedures, as well as benchmark results and evaluations. In terms of datasets, M<sup>2</sup> Hub includes 9 public datasets, such as MP and Carbon24, covering 6 types of materials and involving 56 tasks related to eight material properties.
13. *Phonon DOS Dataset*<sup>200</sup>: The Phonon DOS Dataset contains approximately 1,500 crystalline materials whose phonon DOS is calculated from density functional perturbation theory. Most crystals in the dataset have less than 13 atomic sites per cell.

14. *Carolina Materials Database*<sup>201</sup>: The Carolina Materials Database was created by groups at the University of South Carolina. The database primarily consists of ternary and quaternary materials generated by some AI methods, containing 214,436 inorganic material compounds and over 250,000 calculated properties.
15. *Alexandria Database*<sup>29,202,203</sup>: The Alexandria Database serves as an open-access repository, encompassing DFT-relaxed crystal structures sourced from a wide array of origins. This database includes a large quantity of hypothetical crystal structures generated by ML methods or other methodologies.
16. *Materials Project Trajectory Dataset*<sup>173</sup>: The Materials Project Trajectory Dataset (MPtrj) comprises 1.37 million structure relaxation and static calculation tasks extracted from the MP, employing either the generalized gradient approximation (GGA) or GGA+U exchange correlation. This dataset encompasses 1,580,395 atomic configurations, corresponding energies, 7,944,833 magnetic moments, 49,295,660 force, and 14,223,555 stress.
17. *Quantum MOF*<sup>204</sup>: Quantum MOF (QMOF) is a dataset of over 20K metal-organic frameworks (MOFs) and coordination polymers derived from DFT. The MOFs are all DFT-optimized and are derived from a variety of parent databases, including both experimental and hypothetical MOFs databases.
18. *Open Materials 2024*<sup>22</sup>: The Open Materials 2024 (OMat24) dataset comprises a comprehensive collection of DFT single-point calculations, structural relaxations, and molecular dynamics trajectories across a diverse array of inorganic bulk materials. In total, approximately 118 million structures have been labeled with total energy, atomic forces, and cell stress, with calculations consuming over 400 million core hours of compute resources. The dataset encompasses structures with atom counts ranging from 1 to 100 per structure, with the majority containing 20 atoms or fewer.
19. *SuperCon3D*<sup>133</sup>: SuperCon3D utilizes crystal information, such as chemical composition, space groups, and lattice constants, to match the chemical formulas and critical temperatures ( $T_c$ ) from the SuperCon database<sup>205</sup> with both ordered and disordered crystal structures sourced from the ICSD. The dataset ultimately compiles a collection of 1,578 superconductor materials, each with both  $T_c$  and crystal structure data. Notably, the entirety of the data in SuperCon3D is derived from experimentally validated observations. Furthermore, the dataset includes 83 distinct elements, representing a comprehensive range of elemental types found within the periodic table.
20. *Atomly*<sup>206,207</sup>: The Atomly database provides an extensive collection of material data generated through high-throughput first-principles calculations. This includes 320,000 inorganic crystal structures, 310,000 bandgap and density of states profiles, 12,000 dielectric constant tensors, and 16,000 mechanical tensors. Additionally, the database features derived data on various material properties, such as compound thermodynamic stability, electrode material performance, piezoelectric characteristics, conductivity, effective carrier mass, and a range of other crucial material attributes.

## 6 Conclusions and Future Outlooks

In conclusion, the integration of AI, particularly deep learning, has transformed crystalline material discovery. By leveraging advanced data representations and models such as geometric graph neural networks, transformers, and diffusion models, researchers can predict material properties, synthesize new materials, aid characterization, and accelerate theoretical computations, with exceptional efficiency and accuracy. However, significant challenges remain. In the following section, we will outline future directions to further unlock the potential of AI in this field.

### 6.1 Explainability

To realize the full potential of AI for scientific discovery, AI should not only have prediction and generation abilities but also need explainability. This explainability fosters trust in model outputs, facilitates the validation of scientific hypotheses, and offers actionable insights for refining research investigations, such as optimization for molecular and material structural design<sup>99,208–214</sup>. Toward this goal, many explainable machine learning methods have been proposed recently, and they can be generally classified into two classes: post-hoc methods to explain black-box models and intrinsic methods to create white-box models<sup>215–219</sup>. Post-hoc explainability refers to how a trained model makes predictions, whereas intrinsic interpretability aims to study how to use transparent constituents to construct a model. Despite remarkable progress, the efforts for materials science are relatively limited. In this part, we will outline observations of explainable methods in the context of materials science and provide insights into this field.

Currently, a handful of post-hoc explainability techniques have been devised in materials science. For example, since the attention weights of the transformer reflect the interactions between inputs, Uni-MOF<sup>5</sup> utilizes attention weights as explanations to reveal the interactions between the atom sites of the materials. The derived explanations confirm that chemically linked atoms have strong interactions, which aligns with the chemical intuition. Similarly, SCANN<sup>11</sup> incorporates the attention mechanism

to predict material structure properties and provide meaningful information about the structure-property relationships, where attention scores are used to indicate the importance of each local structure contributing to the accurate prediction.

However, recent studies suggest that "attention is not explanation" because attention weights are often inconsistent with the feature importance<sup>99,220</sup>. Instead of using attention, CrysXPP<sup>221</sup> uses trainable weights of the neural network w.r.t atomic features to indicate the feature importance to the chemical property of the materials. Other works use perturbation based methods to measure the relationship between input features and output<sup>222,223</sup>. The intuition is that perturbing important feature pairs will have a significant impact on model predictions. For instance, CGCNN<sup>23</sup> perturbs each site with different elements, and thus the importance of elements on sites in perovskites to the total energy above hull data can be estimated. However, some studies suggested that generated explanations may change drastically with very small perturbations, and the generated explanations are not robust<sup>223</sup>.

White-box models aim to create interpretable and easily understandable models for humans. Such models include linear, decision tree, and rule-based models. For example, to unravel the correlation between adsorption energy and the properties of the adsorbate-catalyst system, Vinchurkar *et al.*<sup>224</sup> used Shapley additive explanations analysis<sup>225</sup> to provide the top five importance features: adsorbate electronegativity, the number of adsorbate atoms, catalyst electronegativity, effective coordination number, and the sum of atomic numbers of the adsorbate molecule. Based on the features, the rule-based white-box method — symbolic regression<sup>226,227</sup> derives mathematical equations to compute the adsorption energy. These equations provided complimentary to theory equations for adsorption energy calculation. Similarly, Anker *et al.*<sup>228</sup> applied gradient-boosting decision trees to quantify how important each atomic feature in the structure is.

Although these fundamental works have explored interpretability in materials science, many challenges remain unresolved.

1) Explainability granularity: Due to complex and non-linear relationships between material properties and features, material properties can depend on features at different granularity, including atomic, microstructural, and macroscopic structures. However, research on obtaining explanations at various granularities is still very limited.

2) Explainability robustness: Although there are numerous interpretable methods available, such as attention-based, gradient-based, perturbation-based, etc., they may not necessarily produce robust and faithful explanations<sup>99,220,223,229</sup>. In addition, experimental data often contains noise or discrepancy from measurement uncertainties and environmental conditions. In these scenarios, unfaithful explanations could be inferred and result in misleading scientific clues.

3) Interdisciplinary knowledge requirement: Understanding materials science requires knowledge of physics and chemistry, making it challenging to create interpretable models that are accessible to all researchers from different fields. Therefore, relevant benchmarks and ground truth are needed to promote the development of interpretable models in this interdisciplinary.

## 6.2 Self-Driving Laboratories

In materials science, traditional experimental methods often involve researchers manually designing and conducting experiments, which can be time-consuming and labor-intensive<sup>230,231</sup>. In contrast, the recently proposed self-driving or autonomous laboratories use machine learning models to plan and perform experiments, increasing laboratory automation and accelerating the scientific discovery processes<sup>13,232–234</sup>. In this section, we first highlighted representative works on self-driving laboratories and provided further clues.

In these years, self-driving laboratories have covered the automation of retrosynthesis analysis (such as in reinforcement-learning-aided synthesis planning<sup>235,236</sup>), prediction of reaction products (such as in CNNs for reaction prediction<sup>237</sup>) and reaction condition optimization (such as in robotic workflows optimized by active learning<sup>232,238</sup>). Recently, LLMs have provided valuable insights to autonomous driving laboratories, thanks to their extensive knowledge of physics and chemistry, as well as their abilities in chain-of-thought reasoning, self-reflection, and decision-making<sup>239,240</sup>. These LLMs as autonomous agents are typically augmented with tools or action modules, empowering them to directly interact with the physical world, e.g., scientific experimentation<sup>241–243</sup>.

One representative work is ChemCrow<sup>242</sup>. By combining the reasoning power of LLMs with chemical expert knowledge from 18 computational tools in chemistry, ChemCrow showcases one of the first chemistry-related LLM agent interactions with the physical world. ChemCrow has planned and synthesized an insect repellent and three organocatalysts and guided the screening and synthesis of a chromophore with target properties. Jia *et al.* introduced LLMatDesign, a LLM-based framework for materials design<sup>243</sup>. LLMatDesign utilizes LLM agents to translate human instructions, apply modifications to materials, and evaluate outcomes using provided tools. By incorporating self-reflection on its previous decisions, LLMatDesign adapts rapidly to new tasks and conditions in a zero-shot manner. An evaluation of LLMatDesign on several materials design tasks in silico validates LLMatDesign's effectiveness in developing new materials with user-defined target properties in the small data regime.

The pioneering work mentioned above has established the foundational paradigms for self-driving laboratories. However, numerous opportunities remain for further research and development.

1) Human–AI collaboration: First, to prevent self-driving experiments from involving unethical purposes or high-risk

operations, humans must validate AI agents' operations, ensuring they align with accepted scientific principles, safety, and ethical standards<sup>244-246</sup>. Second, experiments often lead to unexpected results that require immediate rethinking and adjustments to protocols. In this scenario, human judgment is invaluable<sup>247-249</sup>. By actively involving human experts in the research loop, their knowledge can be leveraged to inform the design and refinement of experiments, and the interpretation of findings<sup>250-252</sup>. In this aspect, LLMs may play an indispensable role in this "humans in the loop" process, as they provide conversational interfaces that allow researchers to incorporate feedback and human experience.

2) Configurable module integration: Self-driving laboratories should automatically select suitable tools from a wide range of computing and experimental tools and configure them to perform specific tasks<sup>253,254</sup>. Also, the optimal parameters and configurations of these tools should be automatically determined. In addition, for certain experimental processes, such as material screening, many algorithms exist for executing this process. Therefore, it is necessary to conduct algorithm selection to select the most suitable one to perform<sup>255</sup>. These challenges may provide an opportunity for the future development of self-driving laboratories toward standardized operation modes and end-to-end experimental workflows.

3) Material language processing: Knowledge in materials science is often recorded in the form of text language, including not only structured data such as CIFs and SLICES but also non-structured data like literature, descriptions, etc. Therefore, effectively processing and learning these different types of material languages can further unleash the potential of AI in material discovery automation.

### 6.3 Generalizability

Deep learning could suffer from generalizability issues in material science, i.e., their performance on new tasks or unseen data will degrade. To improve the generalizability, one straightforward way is to pre-train on large-scale databases. For example, M3GNet<sup>41</sup> utilizes the largely untapped dataset of more than 187,000 energies, 16,000,000 forces, and 1,600,000 stresses from structural relaxations performed by the Materials Project to train the graph deep learning model. M3GNet showcases the potential generalizability to predict the formation energy, etc, of various materials across the periodic table.

However, pre-training techniques require a large amount of data and computational resources. Furthermore, the distribution of new data may shift from the pre-training data distribution, i.e., out-of-distribution<sup>256</sup>, which could degrade the performance under the new data. In addition to the out-of-distribution caused by new samples, this bias could also stem from the following two aspects: First, crystalline materials can exhibit different behaviors under extreme conditions such as high temperature, pressure, or strain<sup>5</sup>. Models trained on data within normal ranges might fail to generalize to these extreme conditions. Second, crystal defects, such as vacancies, interstitials, or dislocations, introduce variations that might not be adequately captured by models trained on defect-free structures, contributing to the generalizability challenge<sup>33</sup>. To improve the generalizability under out-of-distribution samples, more advanced pretraining techniques<sup>7</sup>, transfer learning<sup>257</sup>, retrieval augmented generation<sup>258</sup>, and zero-shot learning techniques<sup>259</sup> can be developed in the future.

### 6.4 Unified Benchmarking

Though a great number of AI approaches are proposed for various crystalline material discovery tasks, fair assessments are often impeded by inconsistencies in datasets, model architectures, metrics, and other evaluation factors. These inconsistencies could lead to biased evaluations and hinder the creditability of the results. Therefore, there is a pressing need to establish standardized benchmarking protocols across tasks. Fortunately, a handful of efforts have been already made. For example, Geom3D<sup>260</sup>, a platform for geometric modeling on 3D structures, integrates MatBench and QMOF datasets and several geometry neural networks. JARVIS-Leaderboard<sup>261</sup>, an open-source and community-driven platform, allows users to set up benchmarks with various types of input data, such as atomic structures, atomistic images, spectra, and text for several AI-driven tasks including property prediction, force-fields prediction, material generation, etc. However, a wider range of AI approaches, evaluation metrics, and datasets needs to be included to further facilitate benchmarking.

## References

1. Yao, Z. *et al.* Hydrogen radical-boosted electrocatalytic CO<sub>2</sub> reduction using Ni-partnered heteroatomic pairs. *Nat. Commun.* **15**, 9881 (2024).
2. Tsang, C. S. *et al.* Polar and quasicrystal vortex observed in twisted-bilayer molybdenum disulfide. *Science* **386**, 198–205 (2024).
3. Gomes, C. P., Fink, D., Van Dover, R. B. & Gregoire, J. M. Computational sustainability meets materials science. *Nat. Rev. Mater.* **6**, 645–647 (2021).
4. Chanussot\*, L. *et al.* Open catalyst 2020 (oc20) dataset and community challenges. *ACS Catal.* (2021).
5. Wang, J. *et al.* A comprehensive transformer-based approach for high-accuracy gas adsorption predictions in metal-organic frameworks. *Nat. Commun.* **15**, 1904 (2024).

6. Wong, L. W. *et al.* Deciphering the ultra-high plasticity in metal monochalcogenides. *Nat. Mater.* **23**, 196–204 (2024).
7. Vainshtein, B. K. *Fundamentals of crystals: symmetry, and methods of structural crystallography*, vol. 1 (Springer Science & Business Media, 2013).
8. Luo, Y., Liu, C. & Ji, S. Towards symmetry-aware generation of periodic materials. *Adv. Neural Inf. Process. Syst.* **36** (2024).
9. Xie, T., Fu, X., Ganea, O.-E., Barzilay, R. & Jaakkola, T. S. Crystal diffusion variational autoencoder for periodic material generation. In *International Conference on Learning Representations* (2021).
10. Van de Walle, A. A complete representation of structure–property relationships in crystals. *Nat. materials* **7**, 455–458 (2008).
11. Vu, T.-S. *et al.* Towards understanding structure–property relations in materials with interpretable deep learning. *npj Comput. Mater.* **9**, 215 (2023).
12. Liu, Y. *et al.* Experimental discovery of structure–property relationships in ferroelectric materials via active learning. *Nat. Mach. Intell.* **4**, 341–350 (2022).
13. Pyzer-Knapp, E. O. *et al.* Accelerating materials discovery using artificial intelligence, high performance computing and robotics. *npj Comput. Mater.* **8**, 84 (2022).
14. Lan, J. *et al.* Adsorbml: a leap in efficiency for adsorption energy calculations using generalizable machine learning potentials. *npj Comput. Mater.* **9**, 172 (2023).
15. Choudhary, K. *et al.* The joint automated repository for various integrated simulations (jarvis) for data-driven materials design. *npj computational materials* **6**, 173 (2020).
16. Himanen, L., Geurts, A., Foster, A. S. & Rinke, P. Data-driven materials science: status, challenges, and perspectives. *Adv. Sci.* **6**, 1900808 (2019).
17. Chanussot, L. *et al.* The open catalyst 2020 (oc20) dataset and community challenges. *acs catalysis* **11**, 10 (may 2021), 6059–6072 (2021).
18. Tran, R. *et al.* The open catalyst 2022 (oc22) dataset and challenges for oxide electrocatalysts. *ACS Catal.* **13**, 3066–3084 (2023).
19. Goodall, R. E. & Lee, A. A. Predicting materials properties without crystal structure: deep representation learning from stoichiometry. *Nat. communications* **11**, 6280 (2020).
20. Jain, A. *et al.* Commentary: The materials project: A materials genome approach to accelerating materials innovation. *APL materials* **1** (2013).
21. Zitnick, C. L. *et al.* An introduction to electrocatalyst design using machine learning for renewable energy storage. *arXiv preprint arXiv:2010.09435* (2020).
22. Barroso-Luque, L. *et al.* Open materials 2024 (omat24) inorganic materials dataset and models. *arXiv preprint arXiv:2410.12771* (2024).
23. Xie, T. & Grossman, J. C. Crystal graph convolutional neural networks for an accurate and interpretable prediction of material properties. *Phys. review letters* **120**, 145301 (2018).
24. Schütt, K. T., Sauceda, H. E., Kindermans, P.-J., Tkatchenko, A. & Müller, K.-R. Schnet—a deep learning architecture for molecules and materials. *The J. Chem. Phys.* **148** (2018).
25. Chen, C., Ye, W., Zuo, Y., Zheng, C. & Ong, S. P. Graph networks as a universal machine learning framework for molecules and crystals. *Chem. Mater.* **31**, 3564–3572 (2019).
26. Zeni, C. *et al.* A generative model for inorganic materials design. *Nature* 1–3 (2025).
27. Cao, Z., Luo, X., Lv, J. & Wang, L. Space group informed transformer for crystalline materials generation. *arXiv preprint arXiv:2403.15734* (2024).
28. Ye, W., Chen, C., Wang, Z., Chu, I.-H. & Ong, S. P. Deep neural networks for accurate predictions of crystal stability. *Nat. communications* **9**, 3800 (2018).
29. Schmidt, J., Pettersson, L., Verdozzi, C., Botti, S. & Marques, M. A. Crystal graph attention networks for the prediction of stable materials. *Sci. advances* **7**, eabi7948 (2021).
30. Gibson, J., Hire, A. & Hennig, R. G. Data-augmentation for graph neural network learning of the relaxed energies of unrelaxed structures. *npj Comput. Mater.* **8**, 211 (2022).

31. Magar, R., Wang, Y. & Barati Farimani, A. Crystal twins: self-supervised learning for crystalline material property prediction. *npj Comput. Mater.* **8**, 231 (2022).
32. Gu, G. H., Jang, J., Noh, J., Walsh, A. & Jung, Y. Perovskite synthesizability using graph neural networks. *npj Comput. Mater.* **8**, 71 (2022).
33. Ziletti, A., Kumar, D., Scheffler, M. & Ghiringhelli, L. M. Insightful classification of crystal structures using deep learning. *Nat. communications* **9**, 2775 (2018).
34. Yang, S.-H. *et al.* Deep learning-assisted quantification of atomic dopants and defects in 2d materials. *Adv. Sci.* **8**, 2101099 (2021).
35. Choudhary, K. *et al.* Recent advances and applications of deep learning methods in materials science. *npj Comput. Mater.* **8**, 59 (2022).
36. El Mendili, Y. *et al.* Raman open database: first interconnected raman-x-ray diffraction open-access resource for material identification. *J. applied crystallography* **52**, 618–625 (2019).
37. Lee, J.-W., Park, W. B., Lee, J. H., Singh, S. P. & Sohn, K.-S. A deep-learning technique for phase identification in multiphase inorganic compounds using synthetic xrd powder patterns. *Nat. communications* **11**, 86 (2020).
38. Yang, Z. & Buehler, M. J. Linking atomic structural defects to mesoscale properties in crystalline solids using graph neural networks. *Npj Comput. Mater.* **8**, 198 (2022).
39. Pagan, D. C., Pash, C. R., Benson, A. R. & Kasemer, M. P. Graph neural network modeling of grain-scale anisotropic elastic behavior using simulated and measured microscale data. *npj Comput. Mater.* **8**, 259 (2022).
40. Behler, J. & Parrinello, M. Generalized neural-network representation of high-dimensional potential-energy surfaces. *Phys. review letters* **98**, 146401 (2007).
41. Chen, C. & Ong, S. P. A universal graph deep learning interatomic potential for the periodic table. *Nat. Comput. Sci.* **2**, 718–728 (2022).
42. Bartók, A. P., Payne, M. C., Kondor, R. & Csányi, G. Gaussian approximation potentials: The accuracy of quantum mechanics, without the electrons. *Phys. review letters* **104**, 136403 (2010).
43. Batzner, S. *et al.* E (3)-equivariant graph neural networks for data-efficient and accurate interatomic potentials. *Nat. communications* **13**, 2453 (2022).
44. Xiao, H. *et al.* An invertible, invariant crystal representation for inverse design of solid-state materials using generative deep learning. *Nat. Commun.* **14**, 7027 (2023).
45. Han, J., Rong, Y., Xu, T. & Huang, W. Geometrically equivariant graph neural networks: A survey. *arXiv preprint arXiv:2202.07230* (2022).
46. Joshi, C. K., Bodnar, C., Mathis, S. V., Cohen, T. & Lio, P. On the expressive power of geometric graph neural networks. In *International conference on machine learning*, 15330–15355 (PMLR, 2023).
47. Reiser, P. *et al.* Graph neural networks for materials science and chemistry. *Commun. Mater.* **3**, 93 (2022).
48. Naveed, H. *et al.* A comprehensive overview of large language models. *arXiv preprint arXiv:2307.06435* (2023).
49. Chang, Y. *et al.* A survey on evaluation of large language models. *ACM Transactions on Intell. Syst. Technol.* **15**, 1–45 (2024).
50. Cong, S. & Zhou, Y. A review of convolutional neural network architectures and their optimizations. *Artif. Intell. Rev.* **56**, 1905–1969 (2023).
51. Li, Z., Liu, F., Yang, W., Peng, S. & Zhou, J. A survey of convolutional neural networks: analysis, applications, and prospects. *IEEE transactions on neural networks learning systems* **33**, 6999–7019 (2021).
52. Hall, S. R., Allen, F. H. & Brown, I. D. The crystallographic information file (cif): a new standard archive file for crystallography. *Foundations Crystallogr.* **47**, 655–685 (1991).
53. Gruver, N. *et al.* Fine-tuned language models generate stable inorganic materials as text. In *The Twelfth International Conference on Learning Representations* (2024).
54. Chung, S. J., Hahn, T. & Klee, W. Nomenclature and generation of three-periodic nets: the vector method. *Acta Crystallogr. Sect. A: Foundations Crystallogr.* **40**, 42–50 (1984).
55. Eon, J.-G. Euclidian embeddings of periodic nets: definition of a topologically induced complete set of geometric descriptors for crystal structures. *Acta Crystallogr. Sect. A: Foundations Crystallogr.* **67**, 68–86 (2011).

56. Spicher, S. & Grimme, S. Robust atomistic modeling of materials, organometallic, and biochemical systems. *Angewandte Chemie Int. Ed.* **59**, 15665–15673 (2020).
57. Müller, U. & de la Flor, G. *Symmetry relationships between crystal structures: applications of crystallographic group theory in crystal chemistry*, vol. 24 (Oxford University Press, 2024).
58. Tilley, R. J. *Crystals and crystal structures* (John Wiley & Sons, 2020).
59. Ge, B. *et al.* Atomic level defect structure engineering for unusually high average thermoelectric figure of merit in n-type pbse rivalling pbte. *Adv. Sci.* **9**, 2203782 (2022).
60. Jiao, R., Huang, W., Liu, Y., Zhao, D. & Liu, Y. Space group constrained crystal generation. In *The Twelfth International Conference on Learning Representations* (2024).
61. Hahn, T., Shmueli, U. & Arthur, J. W. *International tables for crystallography*, vol. 1 (Reidel Dordrecht, 1983).
62. Janner, A., Janssen, T. & De Wolff, P. Wyckoff positions used for the classification of bravais classes of modulated crystals. *Acta Crystallogr. Sect. A: Foundations Crystallogr.* **39**, 667–670 (1983).
63. Jangid, D. K. *et al.* Q-rbsa: high-resolution 3d ebsd map generation using an efficient quaternion transformer network. *npj Comput. Mater.* **10**, 27 (2024).
64. Robinson, I. & Harder, R. Coherent x-ray diffraction imaging of strain at the nanoscale. *Nat. materials* **8**, 291–298 (2009).
65. Ludwig, W. *et al.* New opportunities for 3d materials science of polycrystalline materials at the micrometre lengthscale by combined use of x-ray diffraction and x-ray imaging. *Mater. Sci. Eng. A* **524**, 69–76 (2009).
66. Zuo, J.-M. *et al.* Data-driven electron microscopy: Electron diffraction imaging of materials structural properties. *Microscopy* **71**, i116–i131 (2022).
67. Kardjilov, N., Manke, I., Woracek, R., Hilger, A. & Banhart, J. Advances in neutron imaging. *Mater. Today* **21**, 652–672 (2018).
68. Bian, K. *et al.* Scanning probe microscopy. *Nat. Rev. Methods Primers* **1**, 36 (2021).
69. Muller, D. A. Structure and bonding at the atomic scale by scanning transmission electron microscopy. *Nat. materials* **8**, 263–270 (2009).
70. Susi, T. *et al.* Isotope analysis in the transmission electron microscope. *Nat. communications* **7**, 13040 (2016).
71. Inkson, B. J. Scanning electron microscopy (sem) and transmission electron microscopy (tem) for materials characterization. In *Materials characterization using nondestructive evaluation (NDE) methods*, 17–43 (Elsevier, 2016).
72. Li, Z., Deng, L., Kinloch, I. A. & Young, R. J. Raman spectroscopy of carbon materials and their composites: Graphene, nanotubes and fibres. *Prog. Mater. Sci.* **135**, 101089 (2023).
73. Cong, X., Liu, X.-L., Lin, M.-L. & Tan, P.-H. Application of raman spectroscopy to probe fundamental properties of two-dimensional materials. *npj 2D Mater. Appl.* **4**, 13 (2020).
74. Han, J. *et al.* A survey of geometric graph neural networks: Data structures, models and applications. *arXiv preprint arXiv:2403.00485* (2024).
75. Wu, F., Wu, L., Radev, D., Xu, J. & Li, S. Z. Integration of pre-trained protein language models into geometric deep learning networks. *Commun. Biol.* **6**, 876 (2023).
76. Atz, K., Grisoni, F. & Schneider, G. Geometric deep learning on molecular representations. *Nat. Mach. Intell.* **3**, 1023–1032 (2021).
77. Gilmer, J., Schoenholz, S. S., Riley, P. F., Vinyals, O. & Dahl, G. E. Neural message passing for quantum chemistry. In *International conference on machine learning*, 1263–1272 (PMLR, 2017).
78. Azimi, S. M., Britz, D., Engstler, M., Fritz, M. & Mücklich, F. Advanced steel microstructural classification by deep learning methods. *Sci. reports* **8**, 2128 (2018).
79. Modarres, M. H. *et al.* Neural network for nanoscience scanning electron microscope image recognition. *Sci. reports* **7**, 13282 (2017).
80. Han, K. *et al.* A survey on vision transformer. *IEEE transactions on pattern analysis machine intelligence* **45**, 87–110 (2022).
81. Xiao, H., Li, L., Liu, Q., Zhu, X. & Zhang, Q. Transformers in medical image segmentation: A review. *Biomed. Signal Process. Control.* **84**, 104791 (2023).

82. Zhang, S. *et al.* Applications of transformer-based language models in bioinformatics: a survey. *Bioinforma. Adv.* **3**, vbad001 (2023).
83. Weininger, D. Smiles, a chemical language and information system. 1. introduction to methodology and encoding rules. *J. chemical information computer sciences* **28**, 31–36 (1988).
84. Zhao, W. X. *et al.* A survey of large language models. *arXiv preprint arXiv:2303.18223* (2023).
85. Delétang, G. *et al.* Language modeling is compression. *arXiv preprint arXiv:2309.10668* (2023).
86. Wu, X., Wu, S.-h., Wu, J., Feng, L. & Tan, K. C. Evolutionary computation in the era of large language model: Survey and roadmap. *arXiv preprint arXiv:2401.10034* (2024).
87. Zhang, Q. *et al.* Scientific large language models: A survey on biological & chemical domains. *arXiv preprint arXiv:2401.14656* (2024).
88. Kenton, J. D. M.-W. C. & Toutanova, L. K. Bert: Pre-training of deep bidirectional transformers for language understanding. In *Proceedings of NAACL-HLT*, 4171–4186 (2019).
89. Zhang, S. *et al.* Opt: Open pre-trained transformer language models. *arXiv preprint arXiv:2205.01068* (2022).
90. Brown, T. *et al.* Language models are few-shot learners. *Adv. neural information processing systems* **33**, 1877–1901 (2020).
91. Touvron, H. *et al.* Llama 2: Open foundation and fine-tuned chat models. *arXiv preprint arXiv:2307.09288* (2023).
92. Chen, Z. *et al.* Meditron-70b: Scaling medical pretraining for large language models. *arXiv preprint arXiv:2311.16079* (2023).
93. Peng, C. *et al.* A study of generative large language model for medical research and healthcare. *NPJ digital medicine* **6**, 210 (2023).
94. Madani, A. *et al.* Progen: Language modeling for protein generation. *arXiv preprint arXiv:2004.03497* (2020).
95. Mansoor, S., Baek, M., Madan, U. & Horvitz, E. Toward more general embeddings for protein design: Harnessing joint representations of sequence and structure. *bioRxiv* 2021–09 (2021).
96. Hwang, Y., Cornman, A. L., Kellogg, E. H., Ovchinnikov, S. & Girguis, P. R. Genomic language model predicts protein co-regulation and function. *Nat. communications* **15**, 2880 (2024).
97. Zhou, G. *et al.* Uni-mol: A universal 3d molecular representation learning framework. *Int. Conf. on Learn. Represent.* (2023).
98. Chang, J. & Ye, J. C. Bidirectional generation of structure and properties through a single molecular foundation model. *Nat. Commun.* **15**, 2323 (2024).
99. Wang, Z. *et al.* Explainable molecular property prediction: Aligning chemical concepts with predictions via language models. *arXiv preprint arXiv:2405.16041* (2024).
100. Beltagy, I., Lo, K. & Cohan, A. Scibert: A pretrained language model for scientific text. In *Proceedings of the 2019 Conference on Empirical Methods in Natural Language Processing and the 9th International Joint Conference on Natural Language Processing (EMNLP-IJCNLP)*, 3615–3620 (2019).
101. Hong, Z. *et al.* The diminishing returns of masked language models to science. In *Findings of the Association for Computational Linguistics: ACL 2023*, 1270–1283 (2023).
102. Briot, J.-P. & Pachet, F. Deep learning for music generation: challenges and directions. *Neural Comput. Appl.* **32**, 981–993 (2020).
103. Creswell, A. *et al.* Generative adversarial networks: An overview. *IEEE signal processing magazine* **35**, 53–65 (2018).
104. Macedo, B., Ribeiro Vaz, I. & Taveira Gomes, T. Medgan: optimized generative adversarial network with graph convolutional networks for novel molecule design. *Sci. Reports* **14**, 1212 (2024).
105. Hong, H., Lin, W. & Tan, K. C. Diffusion-driven domain adaptation for generating 3d molecules. *arXiv preprint arXiv:2404.00962* (2024).
106. Yu, Q. *et al.* A survey on evolutionary computation based drug discovery. *IEEE Transactions on Evol. Comput.* 1–1 (2024).
107. Berahmand, K., Daneshfar, F., Salehi, E. S., Li, Y. & Xu, Y. Autoencoders and their applications in machine learning: a survey. *Artif. Intell. Rev.* **57**, 28 (2024).

108. Ren, Z. *et al.* Inverse design of crystals using generalized invertible crystallographic representation. *arXiv preprint arXiv:2005.07609* **3**, 7 (2020).
109. Goodfellow, I. *et al.* Generative adversarial networks. *Commun. ACM* **63**, 139–144 (2020).
110. Jabbar, A., Li, X. & Omar, B. A survey on generative adversarial networks: Variants, applications, and training. *ACM Comput. Surv. (CSUR)* **54**, 1–49 (2021).
111. Kingma, D., Salimans, T., Poole, B. & Ho, J. Variational diffusion models. *Adv. neural information processing systems* **34**, 21696–21707 (2021).
112. Yang, L. *et al.* Diffusion models: A comprehensive survey of methods and applications. *ACM Comput. Surv.* **56**, 1–39 (2023).
113. Croitoru, F.-A., Hondru, V., Ionescu, R. T. & Shah, M. Diffusion models in vision: A survey. *IEEE Transactions on Pattern Analysis Mach. Intell.* **45**, 10850–10869 (2023).
114. Schütt, K. *et al.* Schnet: A continuous-filter convolutional neural network for modeling quantum interactions. *Adv. neural information processing systems* **30** (2017).
115. Louis, S.-Y. *et al.* Graph convolutional neural networks with global attention for improved materials property prediction. *Phys. Chem. Chem. Phys.* **22**, 18141–18148 (2020).
116. Choudhary, K. & DeCost, B. Atomistic line graph neural network for improved materials property predictions. *npj Comput. Mater.* **7**, 185 (2021).
117. Kaundinya, P. R., Choudhary, K. & Kalidindi, S. R. Prediction of the electron density of states for crystalline compounds with atomistic line graph neural networks (alignn). *JOM* **74**, 1395–1405 (2022).
118. Kaba, O. & Ravanbakhsh, S. Equivariant networks for crystal structures. *Adv. Neural Inf. Process. Syst.* **35**, 4150–4164 (2022).
119. Lin, Y. *et al.* Efficient approximations of complete interatomic potentials for crystal property prediction. In *International Conference on Machine Learning*, 21260–21287 (PMLR, 2023).
120. Das, K. *et al.* Crysgnn: Distilling pre-trained knowledge to enhance property prediction for crystalline materials. In *Proceedings of the AAAI Conference on Artificial Intelligence*, vol. 37, 7323–7331 (2023).
121. Zhong, Y., Yu, H., Gong, X. & Xiang, H. A general tensor prediction framework based on graph neural networks. *The J. Phys. Chem. Lett.* **14**, 6339–6348 (2023).
122. Mao, Z., Li, W. & Tan, J. Dielectric tensor prediction for inorganic materials using latent information from preferred potential. *npj Comput. Mater.* **10**, 265 (2024).
123. Yan, K., Saxton, A., Qian, X., Qian, X. & Ji, S. A space group symmetry informed network for o (3) equivariant crystal tensor prediction. *arXiv preprint arXiv:2406.12888* (2024).
124. Banik, S. *et al.* Cegann: Crystal edge graph attention neural network for multiscale classification of materials environment. *Npj Comput. Mater.* **9**, 23 (2023).
125. Yan, K., Fu, C., Qian, X., Qian, X. & Ji, S. Complete and efficient graph transformers for crystal material property prediction. *arXiv preprint arXiv:2403.11857* (2024).
126. Taniai, T. *et al.* Crystalformer: infinitely connected attention for periodic structure encoding. *arXiv preprint arXiv:2403.11686* (2024).
127. Wang, Y., Kong, S., Gregoire, J. M. & Gomes, C. P. Conformal crystal graph transformer with robust encoding of periodic invariance. In *Proceedings of the AAAI Conference on Artificial Intelligence*, vol. 38, 283–291 (2024).
128. Chen, Z. *et al.* Direct prediction of phonon density of states with euclidean neural networks. *Adv. Sci.* **8**, 2004214 (2021).
129. Lee, N. *et al.* Density of states prediction of crystalline materials via prompt-guided multi-modal transformer. *Adv. Neural Inf. Process. Syst.* **36** (2024).
130. Yan, K., Liu, Y., Lin, Y. & Ji, S. Periodic graph transformers for crystal material property prediction. *Adv. Neural Inf. Process. Syst.* **35**, 15066–15080 (2022).
131. Song, Z., Meng, Z. & King, I. A diffusion-based pre-training framework for crystal property prediction. In *Proceedings of the AAAI Conference on Artificial Intelligence*, vol. 38, 8993–9001 (2024).
132. Kang, Y., Park, H., Smit, B. & Kim, J. A multi-modal pre-training transformer for universal transfer learning in metal–organic frameworks. *Nat. Mach. Intell.* **5**, 309–318 (2023).

133. Chen, P. *et al.* Learning superconductivity from ordered and disordered material structures. In *The Thirty-eight Conference on Neural Information Processing Systems Datasets and Benchmarks Track* (2024).
134. Jain, A., Shin, Y. & Persson, K. A. Computational predictions of energy materials using density functional theory. *Nat. Rev. Mater.* **1**, 1–13 (2016).
135. Li, C.-N., Liang, H.-P., Zhang, X., Lin, Z. & Wei, S.-H. Graph deep learning accelerated efficient crystal structure search and feature extraction. *npj Comput. Mater.* **9**, 176 (2023).
136. Ying, C. *et al.* Do transformers really perform badly for graph representation? *Adv. neural information processing systems* **34**, 28877–28888 (2021).
137. Jiao, R. *et al.* Crystal structure prediction by joint equivariant diffusion on lattices and fractional coordinates. In *Workshop on "Machine Learning for Materials" ICLR 2023* (2023).
138. Chen, R. T., Rubanova, Y., Bettencourt, J. & Duvenaud, D. K. Neural ordinary differential equations. *Adv. neural information processing systems* **31** (2018).
139. Zhao, Y. *et al.* Physics guided deep learning for generative design of crystal materials with symmetry constraints. *npj Comput. Mater.* **9**, 38 (2023).
140. Miller, B. K., Chen, R. T. Q., Sriram, A. & Wood, B. M. FlowMM: Generating materials with riemannian flow matching. In *Forty-first International Conference on Machine Learning* (2024).
141. Gebauer, N., Gastegger, M. & Schütt, K. Symmetry-adapted generation of 3d point sets for the targeted discovery of molecules. *Adv. neural information processing systems* **32** (2019).
142. Ye, C.-Y., Weng, H.-M. & Wu, Q.-S. Con-cdvae: A method for the conditional generation of crystal structures. *Comput. Mater. Today* **1**, 100003 (2024).
143. Luo, X. *et al.* Deep learning generative model for crystal structure prediction. *npj Comput. Mater.* **10**, 254 (2024).
144. Qi, H. *et al.* Latent conservative objective models for data-driven crystal structure prediction. In *AI for Accelerated Materials Design-NeurIPS 2023 Workshop* (2023).
145. Lin, P. *et al.* Equivariant diffusion for crystal structure prediction. In *Forty-first International Conference on Machine Learning* (2024).
146. Klipfel, A., Fregier, Y., Sayede, A. & Bouraoui, Z. Vector field oriented diffusion model for crystal material generation. *Proc. AAAI Conf. on Artif. Intell.* **38**, 22193–22201 (2024).
147. Klipfel, A. *et al.* Equivariant message passing neural network for crystal material discovery. In *AAAI Conference on Artificial Intelligence*, vol. 37, 14304–14311 (2024).
148. Yang, S. *et al.* Scalable diffusion for materials generation. In *The Twelfth International Conference on Learning Representations* (2023).
149. Zhao, Y. *et al.* High-throughput discovery of novel cubic crystal materials using deep generative neural networks. *Adv. Sci.* **8**, 2100566 (2021).
150. Liu, K., Gao, S., Yang, K. & Han, Y. Pcvae: A physics-informed neural network for determining the symmetry and geometry of crystals. In *2023 International Joint Conference on Neural Networks (IJCNN)*, 1–8 (2023).
151. Govindarajan, P. *et al.* Behavioral cloning for crystal design. In *Workshop on "Machine Learning for Materials" ICLR 2023* (2023).
152. Govindarajan, P. *et al.* Learning conditional policies for crystal design using offline reinforcement learning. In *AI for Accelerated Materials Design-NeurIPS 2023 Workshop* (2023).
153. Nguyen, T. M. *et al.* Hierarchical flownet for crystal structure generation. In *AI for Accelerated Materials Design-NeurIPS 2023 Workshop* (2023).
154. Flam-Shepherd, D. & Aspuru-Guzik, A. Language models can generate molecules, materials, and protein binding sites directly in three dimensions as xyz, cif, and pdb files. *arXiv preprint arXiv:2305.05708* (2023).
155. Antunes, L. M., Butler, K. T. & Grau-Crespo, R. Crystal structure generation with autoregressive large language modeling. *Nat. Commun.* **15**, 1–16 (2024).
156. Sriram, A., Miller, B. K., Chen, R. T. & Wood, B. M. Flowllm: Flow matching for material generation with large language models as base distributions. In *The Thirty-eighth Annual Conference on Neural Information Processing Systems* (2024).

157. Yan, K. *et al.* Invariant tokenization of crystalline materials for language model enabled generation. In *The Thirty-eighth Annual Conference on Neural Information Processing Systems*.
158. Yang, S. *et al.* Generative hierarchical materials search. In *The Thirty-eighth Annual Conference on Neural Information Processing Systems*.
159. Sprueill, H. W. *et al.* Chemreasoner: Heuristic search over a large language model's knowledge space using quantum-chemical feedback. *arXiv preprint arXiv:2402.10980* (2024).
160. Batatia, I., Kovacs, D. P., Simm, G., Ortner, C. & Csányi, G. Mace: Higher order equivariant message passing neural networks for fast and accurate force fields. *Adv. Neural Inf. Process. Syst.* **35**, 11423–11436 (2022).
161. Schütt, K., Unke, O. & Gastegger, M. Equivariant message passing for the prediction of tensorial properties and molecular spectra. In *International Conference on Machine Learning*, 9377–9388 (PMLR, 2021).
162. Vignac, C., Loukas, A. & Frossard, P. Building powerful and equivariant graph neural networks with structural message-passing. *Adv. neural information processing systems* **33**, 14143–14155 (2020).
163. Court, C. J., Yildirim, B., Jain, A. & Cole, J. M. 3-d inorganic crystal structure generation and property prediction via representation learning. *J. Chem. Inf. Model.* **60**, 4518–4535 (2020).
164. Castelli, I. E. *et al.* New cubic perovskites for one-and two-photon water splitting using the computational materials repository. *Energy & Environ. Sci.* **5**, 9034–9043 (2012).
165. Dunn, A., Wang, Q., Ganose, A., Dopp, D. & Jain, A. Benchmarking materials property prediction methods: the matbench test set and automatminer reference algorithm. *npj Comput. Mater.* **6**, 138 (2020).
166. Gasteiger, J., Yeshwanth, C. & Günnemann, S. Directional message passing on molecular graphs via synthetic coordinates. *Adv. Neural Inf. Process. Syst.* **34**, 15421–15433 (2021).
167. Gasteiger, J., Becker, F. & Günnemann, S. Gemnet: Universal directional graph neural networks for molecules. *Adv. Neural Inf. Process. Syst.* **34**, 6790–6802 (2021).
168. Jiao, R. *et al.* Crystal structure prediction by joint equivariant diffusion. In Oh, A. *et al.* (eds.) *Advances in Neural Information Processing Systems*, vol. 36, 17464–17497 (Curran Associates, Inc., 2023).
169. Jiao, R., Huang, W., Liu, Y., Zhao, D. & Liu, Y. Space group constrained crystal generation. In *The Twelfth International Conference on Learning Representations* (2023).
170. Stohr, M., Medrano Sandonas, L. & Tkatchenko, A. Accurate many-body repulsive potentials for density-functional tight binding from deep tensor neural networks. *The J. Phys. Chem. Lett.* **11**, 6835–6843 (2020).
171. Ko, T. W., Finkler, J. A., Goedecker, S. & Behler, J. A fourth-generation high-dimensional neural network potential with accurate electrostatics including non-local charge transfer. *Nat. communications* **12**, 398 (2021).
172. Artrith, N. & Urban, A. An implementation of artificial neural-network potentials for atomistic materials simulations: Performance for tio2. *Comput. Mater. Sci.* **114**, 135–150 (2016).
173. Deng, B. *et al.* Chgnet as a pretrained universal neural network potential for charge-informed atomistic modelling. *Nat. Mach. Intell.* **5**, 1031–1041 (2023).
174. Anderson, B., Hy, T. S. & Kondor, R. Cormorant: Covariant molecular neural networks. *Adv. neural information processing systems* **32** (2019).
175. Gasteiger, J., Groß, J. & Günnemann, S. Directional message passing for molecular graphs. In *International Conference on Learning Representations* (2020).
176. Chmiela, S. *et al.* Machine learning of accurate energy-conserving molecular force fields. *Sci. Adv.* **3**, e1603015 (2017).
177. Shui, Z. *et al.* Injecting domain knowledge from empirical interatomic potentials to neural networks for predicting material properties. *Adv. Neural Inf. Process. Syst.* **35**, 14839–14851 (2022).
178. Fu, X. *et al.* Forces are not enough: Benchmark and critical evaluation for machine learning force fields with molecular simulations. *Transactions on Mach. Learn. Res.* (2023).
179. Wang, Z. *et al.* Machine learning method for tight-binding hamiltonian parameterization from ab-initio band structure. *npj Comput. Mater.* **7**, 11 (2021).
180. Agapito, L. A. *et al.* Accurate tight-binding hamiltonians for two-dimensional and layered materials. *Phys. Rev. B* **93**, 125137 (2016).

181. Smutna, J., Fogarty, R., Wenman, M. & Horsfield, A. Systematic development of ab initio tight-binding models for hexagonal metals. *Phys. Rev. Mater.* **4**, 043801 (2020).
182. Koskinen, P. & Mäkinen, V. Density-functional tight-binding for beginners. *Comput. Mater. Sci.* **47**, 237–253 (2009).
183. Elstner, M. & Seifert, G. Density functional tight binding. *Philos. Transactions Royal Soc. A: Math. Phys. Eng. Sci.* **372**, 20120483 (2014).
184. Li, H. *et al.* Deep-learning density functional theory hamiltonian for efficient ab initio electronic-structure calculation. *Nat. Comput. Sci.* **2**, 367–377 (2022).
185. Gu, Q. *et al.* Deep learning tight-binding approach for large-scale electronic simulations at finite temperatures with ab initio accuracy. *Nat. Commun.* **15**, 6772 (2024).
186. Li, H., Collins, C., Tanha, M., Gordon, G. J. & Yaron, D. J. A density functional tight binding layer for deep learning of chemical hamiltonians. *J. chemical theory computation* **14**, 5764–5776 (2018).
187. Gu, Q., Zhang, L. & Feng, J. Neural network representation of electronic structure from ab initio molecular dynamics. *Sci. Bull.* **67**, 29–37 (2022).
188. Li, Y. *et al.* A database of computed raman spectra of inorganic compounds with accurate hybrid functionals. *Sci. Data* **11**, 105 (2024).
189. Park, W. B. *et al.* Classification of crystal structure using a convolutional neural network. *IUCrJ* **4**, 486–494 (2017).
190. Bhattacharya, A., Benavides, J. A., Gerlein, L. F. & Cloutier, S. G. Deep-learning framework for fully-automated recognition of tio2 polymorphs based on raman spectroscopy. *Sci. Reports* **12**, 21874 (2022).
191. Stein, H. S., Soedarmadji, E., Newhouse, P. F., Guevarra, D. & Gregoire, J. M. Synthesis, optical imaging, and absorption spectroscopy data for 179072 metal oxides. *Sci. data* **6**, 9 (2019).
192. Saal, J. E., Kirklin, S., Aykol, M., Meredig, B. & Wolverton, C. Materials design and discovery with high-throughput density functional theory: the open quantum materials database (oqmd). *Jom* **65**, 1501–1509 (2013).
193. Kirklin, S. *et al.* The open quantum materials database (oqmd): assessing the accuracy of dft formation energies. *npj Comput. Mater.* **1**, 1–15 (2015).
194. Pickard, C. J. Airss data for carbon at 10gpa and the c+n+h+o system at 1gpa (2020).
195. Vaitkus, A., Merkys, A. & Gražulis, S. Validation of the crystallography open database using the crystallographic information framework. *J. applied crystallography* **54**, 661–672 (2021).
196. Bergerhoff, G., Brown, I., Allen, F. *et al.* Crystallographic databases. *Int. Union Crystallogr. Chester* **360**, 77–95 (1987).
197. Zagorac, D., Müller, H., Ruehl, S., Zagorac, J. & Rehme, S. Recent developments in the inorganic crystal structure database: theoretical crystal structure data and related features. *J. applied crystallography* **52**, 918–925 (2019).
198. Ong, S. P. *et al.* Python materials genomics (pymatgen): A robust, open-source python library for materials analysis. *Comput. Mater. Sci.* **68**, 314–319 (2013).
199. Du, Y. *et al.* M<sup>2</sup> hub: Unlocking the potential of machine learning for materials discovery. *Adv. Neural Inf. Process. Syst.* **36**, 77359–77378 (2023).
200. Petretto, G. *et al.* High-throughput density-functional perturbation theory phonons for inorganic materials. *Sci. data* **5**, 1–12 (2018).
201. Zhao, Y. *et al.* High-throughput discovery of novel cubic crystal materials using deep generative neural networks. *Adv. Sci.* **8**, 2100566 (2021).
202. Schmidt, J. *et al.* Large-scale machine-learning-assisted exploration of the whole materials space. *arXiv preprint arXiv:2210.00579* (2022).
203. Schmidt, J. *et al.* Machine-learning-assisted determination of the global zero-temperature phase diagram of materials. *Adv. Mater.* **35**, 2210788 (2023).
204. Rosen, A. S. *et al.* Machine learning the quantum-chemical properties of metal–organic frameworks for accelerated materials discovery. *Matter* **4**, 1578–1597 (2021).
205. Stanev, V. *et al.* Machine learning modeling of superconducting critical temperature. *npj Comput. Mater.* **4**, 29 (2018).
206. Atomly, <https://atomly.net> (2020).

207. Yu, Z. *et al.* Superconductive materials with mgb 2-like structures from data-driven screening. *Phys. Rev. B* **105**, 214517 (2022).
208. Lin, W., Lan, H. & Li, B. Generative causal explanations for graph neural networks. In *International Conference on Machine Learning*, 6666–6679 (PMLR, 2021).
209. Lin, W., Lan, H., Wang, H. & Li, B. Orphicx: A causality-inspired latent variable model for interpreting graph neural networks. In *Proceedings of the IEEE/CVF Conference on Computer Vision and Pattern Recognition*, 13729–13738 (2022).
210. Gallegos, M., Vassilev-Galindo, V., Poltavsky, I., Martín Pendás, Á. & Tkatchenko, A. Explainable chemical artificial intelligence from accurate machine learning of real-space chemical descriptors. *Nat. Commun.* **15**, 4345 (2024).
211. Deng, J. *et al.* A systematic study of key elements underlying molecular property prediction. *Nat. Commun.* **14**, 6395 (2023).
212. Kim, C. *et al.* Transparent medical image ai via an image–text foundation model grounded in medical literature. *Nat. Medicine* 1–12 (2024).
213. Ying, Z., Bourgeois, D., You, J., Zitnik, M. & Leskovec, J. Gnnexplainer: Generating explanations for graph neural networks. *Adv. neural information processing systems* **32** (2019).
214. Fang, J. *et al.* Cooperative explanations of graph neural networks. In *Proceedings of the Sixteenth ACM International Conference on Web Search and Data Mining*, 616–624 (2023).
215. Turbé, H., Bjelogrić, M., Lovis, C. & Mengaldo, G. Evaluation of post-hoc interpretability methods in time-series classification. *Nat. Mach. Intell.* **5**, 250–260 (2023).
216. Linardatos, P., Papastefanopoulos, V. & Kotsiantis, S. Explainable ai: A review of machine learning interpretability methods. *Entropy* **23**, 18 (2020).
217. Fang, J. *et al.* On regularization for explaining graph neural networks: An information theory perspective. *IEEE Transactions on Knowl. Data Eng.* 1–14 (2024).
218. Huang, Q., Yamada, M., Tian, Y., Singh, D. & Chang, Y. Graphlime: Local interpretable model explanations for graph neural networks. *IEEE Transactions on Knowl. Data Eng.* (2022).
219. Vu, M. & Thai, M. T. Pgm-explainer: Probabilistic graphical model explanations for graph neural networks. *Adv. neural information processing systems* **33**, 12225–12235 (2020).
220. Serrano, S. & Smith, N. A. Is attention interpretable? In *Proceedings of the 57th Annual Meeting of the Association for Computational Linguistics*, 2931–2951 (2019).
221. Das, K. *et al.* Crysxpp: An explainable property predictor for crystalline materials. *npj Comput. Mater.* **8**, 43 (2022).
222. Fel, T. *et al.* Don't lie to me! robust and efficient explainability with verified perturbation analysis. In *Proceedings of the IEEE/CVF Conference on Computer Vision and Pattern Recognition*, 16153–16163 (2023).
223. Agarwal, S. *et al.* Towards the unification and robustness of perturbation and gradient based explanations. In *International Conference on Machine Learning*, 110–119 (PMLR, 2021).
224. Vinchurkar, T., Ock, J. & Farimani, A. B. Explainable data-driven modeling of adsorption energy in heterogeneous catalysis (2024).
225. Lundberg, S. M. & Lee, S.-I. A unified approach to interpreting model predictions. *Adv. neural information processing systems* **30** (2017).
226. Wang, Y., Wagner, N. & Rondinelli, J. M. Symbolic regression in materials science. *MRS Commun.* **9**, 793–805 (2019).
227. Makke, N. & Chawla, S. Interpretable scientific discovery with symbolic regression: a review. *Artif. Intell. Rev.* **57**, 2 (2024).
228. Anker, A. S. *et al.* Extracting structural motifs from pair distribution function data of nanostructures using explainable machine learning. *npj Comput. Mater.* **8**, 213 (2022).
229. Rudin, C. Stop explaining black box machine learning models for high stakes decisions and use interpretable models instead. *Nat. machine intelligence* **1**, 206–215 (2019).
230. Cawse, J. N. *Experimental design for combinatorial and high throughput materials development* (Citeseer, 2003).
231. Talapatra, A. *et al.* Autonomous efficient experiment design for materials discovery with bayesian model averaging. *Phys. Rev. Mater.* **2**, 113803 (2018).

232. Burger, B. *et al.* A mobile robotic chemist. *Nature* **583**, 237–241 (2020).
233. Xie, Y., Sattari, K., Zhang, C. & Lin, J. Toward autonomous laboratories: Convergence of artificial intelligence and experimental automation. *Prog. Mater. Sci.* **132**, 101043 (2023).
234. Seifrid, M. *et al.* Autonomous chemical experiments: Challenges and perspectives on establishing a self-driving lab. *Accounts Chem. Res.* **55**, 2454–2466 (2022).
235. Segler, M. H., Preuss, M. & Waller, M. P. Planning chemical syntheses with deep neural networks and symbolic ai. *Nature* **555**, 604–610 (2018).
236. Coley, C. W. *et al.* A robotic platform for flow synthesis of organic compounds informed by ai planning. *Science* **365**, eaax1566 (2019).
237. Coley, C. W. *et al.* A graph-convolutional neural network model for the prediction of chemical reactivity. *Chem. science* **10**, 370–377 (2019).
238. Granda, J. M., Donina, L., Dragone, V., Long, D.-L. & Cronin, L. Controlling an organic synthesis robot with machine learning to search for new reactivity. *Nature* **559**, 377–381 (2018).
239. Ramos, M. C., Collison, C. & White, A. D. A review of large language models and autonomous agents in chemistry. *Chem. Sci.* (2024).
240. Liu, Z. *et al.* Bolaa: Benchmarking and orchestrating llm-augmented autonomous agents. *arXiv preprint arXiv:2308.05960* (2023).
241. Miret, S. & Krishnan, N. Are llms ready for real-world materials discovery? *arXiv preprint arXiv:2402.05200* (2024).
242. M. Bran, A. *et al.* Augmenting large language models with chemistry tools. *Nat. Mach. Intell.* 1–11 (2024).
243. Jia, S., Zhang, C. & Fung, V. Llm4design: Autonomous materials discovery with large language models. *arXiv preprint arXiv:2406.13163* (2024).
244. Biswas, A. & Talukdar, W. Guardrails for trust, safety, and ethical development and deployment of large language models (llm). *J. Sci. & Technol.* **4**, 55–82 (2023).
245. Ji, J. *et al.* Beavertails: Towards improved safety alignment of llm via a human-preference dataset. *Adv. Neural Inf. Process. Syst.* **36** (2024).
246. Yao, Y. *et al.* A survey on large language model (llm) security and privacy: The good, the bad, and the ugly. *High-Confidence Comput.* 100211 (2024).
247. Liu, S. *et al.* Conversational drug editing using retrieval and domain feedback. In *The Twelfth International Conference on Learning Representations* (2023).
248. Drori, I. & Te'eni, D. Human-in-the-loop ai reviewing: Feasibility, opportunities, and risks. *J. Assoc. for Inf. Syst.* **25**, 98–109 (2024).
249. Huang, S.-H. *et al.* On replacing humans with large language models in voice-based human-in-the-loop systems. In *Proceedings of the AAAI Symposium Series*, vol. 3, 45–49 (2024).
250. Liu, Z. *et al.* Machine learning with knowledge constraints for process optimization of open-air perovskite solar cell manufacturing. *Joule* **6**, 834–849 (2022).
251. Tiihonen, A. *et al.* More trustworthy bayesian optimization of materials properties by adding human into the loop. In *AI for Accelerated Materials Design NeurIPS 2022 Workshop* (2022).
252. Sun, S. *et al.* A data fusion approach to optimize compositional stability of halide perovskites. *Matter* **4**, 1305–1322 (2021).
253. Abolhasani, M. & Kumacheva, E. The rise of self-driving labs in chemical and materials sciences. *Nat. Synth.* **2**, 483–492 (2023).
254. Kannan, J. Can llms configure software tools. *arXiv preprint arXiv:2312.06121* (2023).
255. Kerschke, P., Hoos, H. H., Neumann, F. & Trautmann, H. Automated algorithm selection: Survey and perspectives. *Evol. computation* **27**, 3–45 (2019).
256. Omeo, S. S., Fu, N., Dong, R., Hu, M. & Hu, J. Structure-based out-of-distribution (ood) materials property prediction: a benchmark study. *npj Comput. Mater.* **10**, 144 (2024).
257. Niu, S., Liu, Y., Wang, J. & Song, H. A decade survey of transfer learning (2010–2020). *IEEE Transactions on Artif. Intell.* **1**, 151–166 (2020).

258. Gao, Y. *et al.* Retrieval-augmented generation for large language models: A survey. *arXiv preprint arXiv:2312.10997* (2023).
259. Song, Y., Wang, T., Cai, P., Mondal, S. K. & Sahoo, J. P. A comprehensive survey of few-shot learning: Evolution, applications, challenges, and opportunities. *ACM Comput. Surv.* **55** (2023).
260. Liu, S. *et al.* Symmetry-informed geometric representation for molecules, proteins, and crystalline materials. *Adv. Neural Inf. Process. Syst.* **36** (2024).
261. Choudhary, K. *et al.* Jarvis-leaderboard: a large scale benchmark of materials design methods. *npj Comput. Mater.* **10**, 93 (2024).